

Article

Mortars and Renders: The Case of the Roman Villa Horta da Torre Fronteira, Portugal

A. Ditta ^{1,2,*} , André Carneiro ³, Cristina Galacho ⁴  and Patrícia Moita ⁵

¹ School of Architecture, Southeast University, 2 Sipailou, Nanjing 210096, China

² School of Architecture & Planning, University of Management & Technology, Lahore 54770, Pakistan

³ CHAIA-UÉ, CECH-FLUC, Department of History, University of Évora, Rua do Cardeal Rei, s/n, 7000-849 Évora, Portugal; ampc@uevora.pt

⁴ Chemistry and Biochemistry Department, HERCULES Laboratory, In2Past, Associated Laboratory, School of Sciences and Technology, University of Évora, Rua do Cardeal Rei, s/n, 7000-849 Évora, Portugal; pcg@uevora.pt

⁵ Geosciences Department, HERCULES Laboratory, In2Past, Associated Laboratory, School of Sciences and Technology, University of Évora, Rua do Cardeal Rei, s/n, 7000-849 Évora, Portugal; pmoita@uevora.pt

* Correspondence: ad.ar26@hotmail.com

Abstract: The archaeological site of *villa* Horta da Torre in Portugal reveals distinctive architectural features within the context of Roman *villae* in Hispania. Notably, the *triclinium* was designed with an artificial cascade originating from a double apse wall, and the walls were adorned with mosaic *tessellae* panels and marble skirting. During the Roman era, the surrounding area belonged to the former province of *Lusitania*, with *Augusta Emerita* serving as its capital. This study examines 11 mortar samples from various contexts and functions, such as masonry, preparatory, render, and *opus signinum* mortars. A set of complementary analytical techniques was employed to determine the textural and mineralogical compositions of the mortars. The aim was to gain insights into the production techniques and the selection of raw materials within the geological context of this rural construction. It was observed that the processing of raw materials and production techniques did not always adhere to the rules of Vitruvius. A comparison with other villas revealed comparatively less meticulous attention to sand selection and precise layering for mural painting. Nevertheless, it was noted that in preparatory layers for the *supranucleus* and *nucleus* tesserae, ceramic pieces were intentionally added to improve the mortar. The binder used was calcitic lime, likely obtained from locally sourced limestone. The nature of aggregates is diversified but consistent with the local geological provenance within a radius of less than 3 km, in accordance with two sand exploration sites. This research aligns with the United Nations' 2030 Agenda for Sustainable Development, contributing specifically to SDG 11 and Target 11.4, which "aims to strengthen efforts to protect and safeguard the world's cultural and natural heritage".

Keywords: Horta da Torre; Roman mortars; characterization; provenance; VP-SEM-EDS; XRD; TGA; multi-analytical approach



Citation: Ditta, A.; Carneiro, A.; Galacho, C.; Moita, P. Mortars and Renders: The Case of the Roman Villa Horta da Torre Fronteira, Portugal. *Heritage* **2024**, *7*, 1589–1617. <https://doi.org/10.3390/heritage7030076>

Academic Editor: João Pedro Veiga

Received: 28 December 2023

Revised: 28 February 2024

Accepted: 29 February 2024

Published: 14 March 2024



Copyright: © 2024 by the authors. Licensee MDPI, Basel, Switzerland. This article is an open access article distributed under the terms and conditions of the Creative Commons Attribution (CC BY) license (<https://creativecommons.org/licenses/by/4.0/>).

1. Introduction

During a visit to any monument, regardless of its historical period, mortars often do not visually stand out or immediately captivate observers. Unless they are supporting mural paintings, in the absence of such associations, mortars may fail to leave a lasting impression on visitors. However, it is essential to acknowledge the pivotal roles mortars play in the sustainability, conservation, and beautification of buildings. A multidisciplinary study of mortars enables a comprehensive understanding of construction techniques employed across different historical periods and the influence of surrounding geological territory on the selection of raw materials, options, and decisions made by ancient civilizations. In early human history, mud served as a mortar, plastering mixture, and a fundamental construction

material for shelters worldwide [1,2]. The earliest documented use of lime as a medium for painting wall surfaces in architectural practices dates back to the fourth millennium BCE in Palestine and Anatolia [3]. Furthermore, mortar technology is believed to have originated in the Middle East, spread to the Greeks, and was subsequently adopted and refined by the Romans [1,4], marking a significant advancement in construction practices.

Lime mortar, a mixture of lime, sand, and water, has been produced and utilized in construction since ancient times [5–7]. In his work ‘*De Architectura*’ or ‘Ten Books on Architecture’, the Roman architectural historian P. Vitruvius discussed various functional mortars, including water proofing, filling, or rendering mortars [1,2,8–10]. Characteristics such as differences in aggregate grain size, the lime-to-aggregate ratio, and the use of additives provide insights into their intended functionality and the care taken in their preparation. Additionally, changes in raw materials may be linked to different construction phases or building technologies [11–13].

This study performed a comprehensive characterization and analysis of the mortars from the Roman *villa* Horta da Torre. It aims to understand the processing of materials and manufacturing technology involved, contributing valuable data to support chronological relationships. The study also seeks to comprehend builders’ perceptions and knowledge of their surroundings by proposing the geological provenance of the raw materials. Furthermore, for preservation and potential museum display, the use of compatible materials is crucial to maintain the aesthetics and consistency of the original construction materials.

The archaeological site of the Roman *villa* Horta da Torre is situated near Cabeço de Vide in the municipality of Fronteira, within the Alentejo region of central Portugal (Figure 1a). It is approximately 130 km away from the Roman capital city of Mérida (*Augustus Emerita*), in the Lusitania province of Spain (Figure 1b). The *villa* occupies a strategic position within the southwest Lusitania and north Baetica territories, as depicted in Figure 1c. The *villa* features a monumental display built in the middle of the third century and was abandoned in the early fifth century. Subsequent occupations have left evidence recovered during excavation processes that allows us to state that this *villa* is one of the best-documented sites in Portugal for understanding the “end of the *villae*” process [14]. Archaeological excavations initiated in 2012 have revealed the *pars urbana*, while the *pars rustica* still remains to be excavated. Despite continued occupations, the large, monumental *villa* has remained well-preserved, displaying unique architectural and aesthetic characteristics within the context of the Roman *villae* in Hispania.

The significance of this settlement network is underscored by three primary routes connecting the provincial capital, *Augusta Emerita*, to its Atlantic port, *Olisipo* (modern day Lisbon), shown in Figure 1d. Notably, Horta da Torre distinguishes itself by featuring the only known *stibadium* south of the river Tagus and because of its unique characteristics in the decorative program of this environment, documented through archaeological excavations.

Two principal routes, via Augusta and via Emerita, passed near the *villa* Horta da Torre in the Hispania region. The former served as a significant east–west route, linking various cities and settlements (Figure 1d) and facilitating trade, communication, and military movements. The route via Emerita Augusta was connected to other Lusitanian cities by the route via Emerita [15]. Furthermore, it played a pivotal role in connecting the Roman Empire to interior regions such as Horta da Torre. This road likely served as an important trade and communication artery during the Roman period, facilitating the flow of people, goods, and ideas between these two regions.

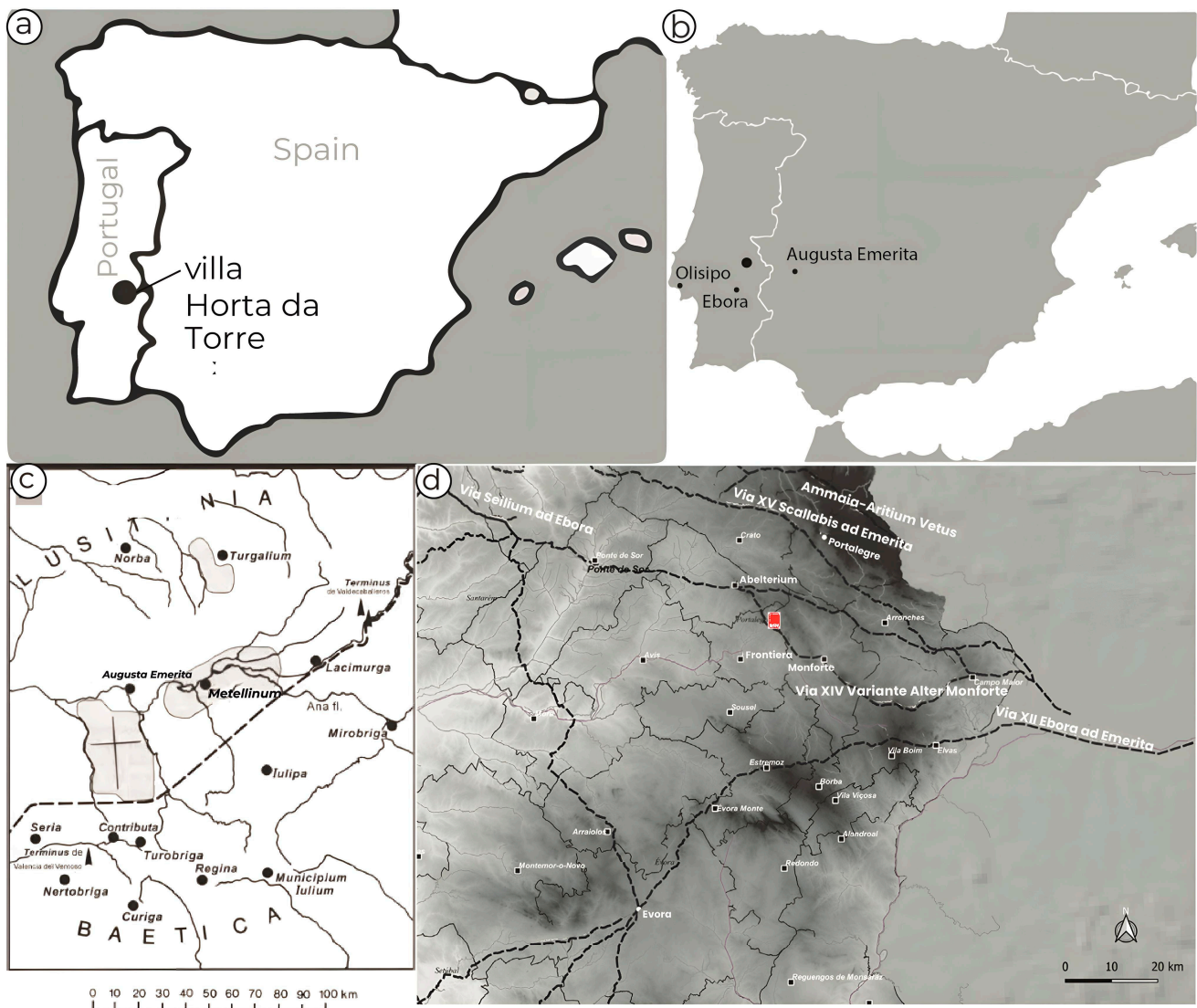


Figure 1. (a): Picture showing the approximate location of the Roman *villa* of Horta da Torre in the Iberian Peninsula; (b) showing the territory of Emerita, Eborā, and Olisipo; (c) map of southwest Lusitania and north Baetica, showing the territory of Emerita due south of the colony (marked with a cross) and the territory of Metellinum ([15,16] credit Edmondson 2011: 33, fig. 3.1); (d) location of the *villa* (marked in red) in the Roman road network in the Alto Alentejo (adapted from Jesus García Sánchez).

The *villa* featured a spacious reception room, the *triclinium*, for hosting guests. It had an area of about 90 m² (Figure 2a) and was situated on its northern side. Adjacent to it, there is a double apse structure interpreted as a water reservoir positioned behind the *stibadium* (Figure 2b). As a decorative eccentricity, the *triclinium* had an artificial cascade originating from the apse's wall that would offer a playful water system covering its floor. The *triclinium* walls were adorned with mosaic *tessellae* panels, while the skirting was covered with marble slabs (Figure 2c). Mural paintings were preserved in the small *peristylum* (Figure 2d). The unique indoor environment of the *villa*, sophisticated technical interventions, and ornate decorations collectively contributed to an impressive ambiance that was undoubtedly enjoyed by the distinguished guests invited by the affluent owner of the *villa* [17,18].



Figure 2. An overview of the different parts of the site: (a) a perspective view of the main banquet hall (i.e., *triclinium*); (b) walls of the double apse (abside) structure; (c) marble cladding working as a skirting, filling mortar layer and the structural wall is visible; (d) survived part of the mural painting from inside the room.

The *villa* Horta da Torre, situated within Hispania, lies to the west of Mérida and in close proximity to the main road linking Mérida to Lisbon. The *villa* is located in an area renowned for hosting one of the largest concentrations of *villae* in all of Hispania [18,19]. The study holds significance due to its distinctive architectural features; including wall mosaics, double abside structures, and a water reservoir. Despite its rural setting and distance from the Empire's central hubs, its strategic proximity to an important commercial route makes it a pertinent case study. This investigation aims to contribute to the understanding of construction techniques, the rules of mixing mortar constituents, and the choices made by the wealthy owner of the *villa*.

Geological Context

The Roman *villa* is located within the geological context of the so-called Iberian Massif, specifically in the Ossa–Morena Zone. The black star on Figure 3 indicates the approximate location of the *villa*. This broad area is characterized by a diverse range of igneous and metamorphic rocks (Figure 3), predominantly oriented in a northwest–southeast (NW–SE) direction, roughly perpendicular to the flow of water lines into the southwest (SW). In detail, the *villa* was built on a geological substrate of metamorphic rocks, including schists, quartzites, and greywakes that outcrop in its vicinity. Other than the metamorphic rocks, to the north lies an igneous ultrabasic and basic intrusion, partially serpentinized, known as the Alter do Chão intrusion. This elongated intrusion aligns with the Variscan structure, which began a contact aureole in the regional limestone and dolostone. Further southwest, a calc-alkaline granite intersects the regional metamorphic rocks.

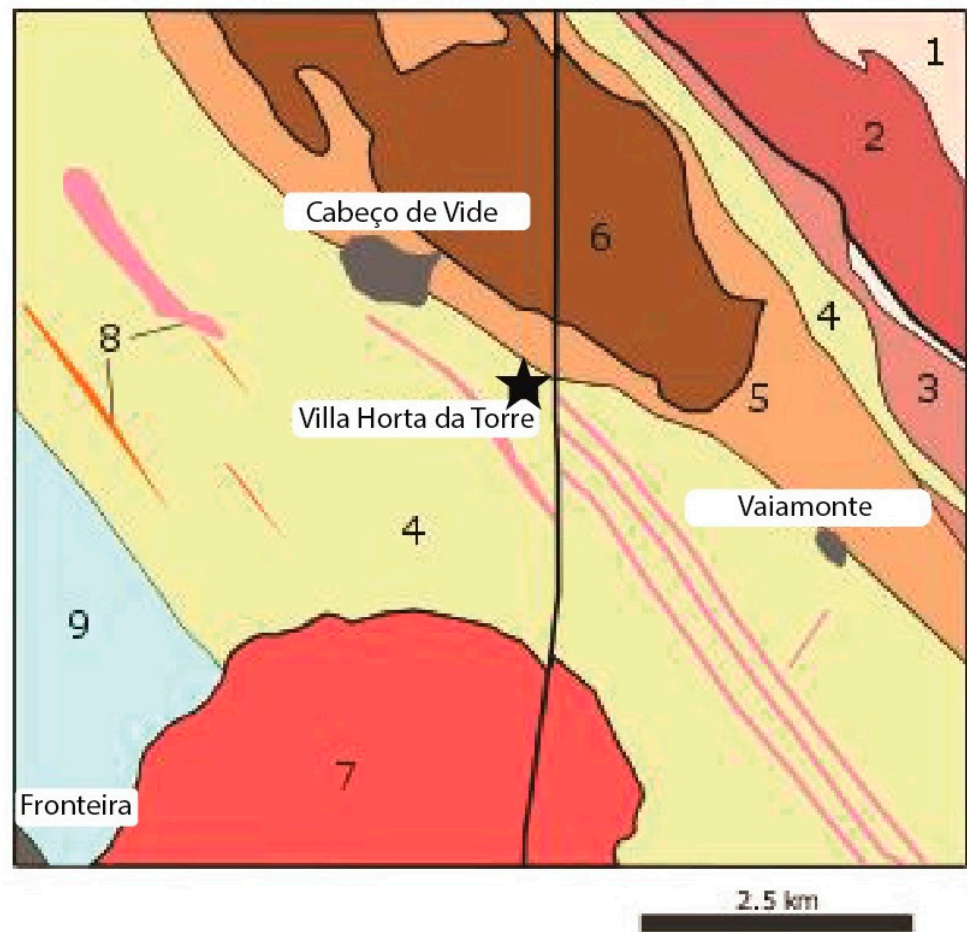


Figure 3. Simplified geological map of the *villa* Horta da Torre extracted and adapted from geological map 32-B (Sousel) and 32-B (Portalegre) at a scale of 1:50,000 (both Gonçalves, 1973). Numbers correspond to the following: 1—shists and greywackes; 2—biotitic granite orthogneiss; 3—hyperalkaline granitic or syenitic orthogneiss; 4—conglomerates and arkoses; 5—hornfels (quartzitic, pelitic, and calcosilicate); 6—ultrabasic-basic intrusion of Alter do Chão; 7—crystalline limestones; 8—schists, quartzite and grauwaques; 9—granitic dykes.

Extending from the northeast (N-E) to the southwest (S-W) and encompassing Horta da Torre, the water lines sequentially traverse shists and greywackes, orthogneisses, hyperalkaline granitic or syenitic orthogneisses, conglomerates and arkoses, the aforementioned intrusion of Alter do Chão surrounded by hornfels (quartzitic, pelitic and calcosilicate), crystalline limestone and dolostone, and culminating in the unit where the Roman *villa* is situated. This entire sequence is intersected by a north–south fault passing approximately 500 m east of the archaeological excavation site. The nearest stream, the Verdigão stream, located 100–200 m away, flows from N-E to S-W with an intense flow, even during the summer season.

2. Materials and Methods

In this research, mortar and render samples from different contexts and functions within *villa* Horta da Torre were fully characterized using a well-established methodology [7,13]. Following registration and physical sample preparation, a suite of complementary analytical techniques was employed, including stereomicroscopy, optical microscopy (OM), variable pressure scanning electron microscopy coupled with energy dispersive spectroscopy (VP-SEM-EDS), X-ray powder diffraction (XRD), and thermogravimetric analysis (TGA). These methodologies collectively facilitated the determination of the

textural, mineralogical, and chemical composition [7] of different types of mortars obtained from the *villa*.

2.1. Samples

Eleven mortar samples were collected from distinct locations within *villa* Horta da Torre, corresponding to their specific functions in the building (refer to Figure 4 for extraction points). Notably, HT-13P and HT-16P were painting/rendering mortars used for mural paintings in the peristyle. HT-18 and HT-19 served as masonry mortars extracted from the inner apse and outer apse, respectively. HT-31A and HT-40B were obtained from the narrow south wall and wider north wall, respectively, both designated for masonry purposes. HT-60 was collected from the water tank wall and was also intended for masonry applications. For specialized applications, HT-20T was sourced from the ceiling above the *stibadium*, and HT-22T originated from the southwest wall of the *triclinium*. Both mortars were utilized as preparative materials for wall mosaic tesserae. Additionally, HT-31B, extracted from the narrow south wall, and HT-40A, extracted from the wider north wall, served as filling material between the wall and marble (slab) cladding. This categorization and extraction information provides a comprehensive insight into the diverse mortars utilized in various architectural elements of the *villa*. Sample collection was conducted under the guidance of an authorized archaeologist, with prior approval from the municipality of Fronteira, Portugal.



Figure 4. Aerial view of the archaeological site of Roman *villa* Horta da Torre in Alentejo, Portugal, highlighting sample extraction locations for the study. (Photo credit: Geo-Drone).

2.2. Sample Preparation

Each mortar sample underwent meticulous cleaning with a scalpel and was brushed to remove dust and biological colonization. Samples were then individually prepared for various laboratory analyses, following the specific requirements of the equipment used. In cases where stratigraphy was present, distinct mortar layers were mechanically separated using a chisel and rubber hammer to create a global fraction (G.F) consisting of both aggregate and binder. Subsequently, the separated layers were mashed to approximately 5 mm using an agate and pestle, followed by further grinding in a RETSCH PM100 Ball Mill adjusted to 500 rotations per minute for 10 min to obtain a fine powder fraction. Grinding

was repeated under the same conditions as necessary to achieve the desired fine powder consistency suitable for XRD and TGA analysis.

2.3. Instrumental Methods

Preliminary macroscopic observations, including visual examination with the unaided eye and photographs taken with a digital camera (model Infinity X from DeltaPix Smorum, Denmark), were conducted to document the mortar composition and characteristics such as the nature of aggregates with respect to their color, size and angular morphology. Polished sections of mortar samples were then observed under a Leica M205C stereo-zoom microscope to examine characteristics such as stratigraphy, binder composition, presence of lime lumps, and spatial distribution of mortar components. Specific petrographic observations of thin sections and corresponding photographic documentation were obtained using a dark-field microscope (Leica DM2500P) at magnifications of 100X and 200X, equipped with a Leica DFC 290HD camera.

The mineralogical composition of crystalline phases in the samples was determined with X-ray powder diffraction (XRD) using the D8 Discover BRUKER X-Ray Diffractometer. The instrument (XRD) utilized a Cu K α source operating at 40 kV and 40 mA, along with a LYNXEYE linear detector. Diffractograms were collected within a 2 θ angular range of 3–75°, employing a step size of 0.05° and a measuring time of 5 s per step. Identification of crystalline phases was performed using the Bruker EVA software version 5.1.0.5 (32 bit) package (DIFFRAC.SUITE EVA, database: ICDD PDF-2).

Thermogravimetric analysis (TGA) is an essential technique for mortar studies as it allows estimation of the binder nature and determination of its thermal stability. Thermal analysis was performed on global fractions (25 to 30 mg, inserted into a platinum crucible) of all mortar samples. Thermal transformations of all the samples were performed using the NETZSCH STA 449F3 Jupiter analyzer under an inert nitrogen atmosphere (Air Liquid Alphagaz compressed N₂) with a flow rate of 70 mL/min. The heating program followed a linear velocity, increasing at a rate of 10 °C/min, starting from 40 °C until reaching 1000 °C. Quantitative analysis of TGA curves (percent weight loss versus temperature) was carried out using Netzsch Proteus 61 software version 6.1.0 (11 July 2014) within selected temperature ranges.

For elemental analysis and determination of aggregates and binder composition, variable pressure scanning electron microscopy-energy dispersive spectroscopy (VP-SEM-EDS) with a low vacuum system was employed. Polished and thin sections were observed in SEM-EDS to comprehend the morphology, neo-formations, and degradation products. Analyses were conducted using a Hitachi S-3700N variable pressure scanning electron microscope coupled with a Bruker Xflash 5010 X-ray energy dispersive spectrometer under a pressure of 40 Pa. Imaging and chemical analyses were conducted in a vacuum chamber with an acceleration voltage of 20.0 kV. Backscattered electron (BSE) mode was utilized for SEM imaging, while EDX tasks and quantification were performed using Esprit 1.8 software from Bruker.

3. Results

3.1. Macroscopic and Stereomicroscopic Observations

This section provides detailed macroscopic and stereomicroscopic observations of mortar samples collected from various locations, systematically categorized into four groups based on their functions. The above Figure 4 illustrates the locations of the extracted samples, while the Figure 5 visually represents the different mortar groups. Group 1 (G-1; Figure 5a) comprises wall painting mortar samples with a chromatic layer. Group 2 (G-2; Figure 5b) includes preparation mortars for wall mosaic tesserae (*opus sectile*). Group 3 (G-3; Figure 5c) consists of filling or preparation mortars located between walls and marble slabs or wall skirtings. Group 4 (G-4; Figure 5d) comprises masonry mortars used for joining stone layers.

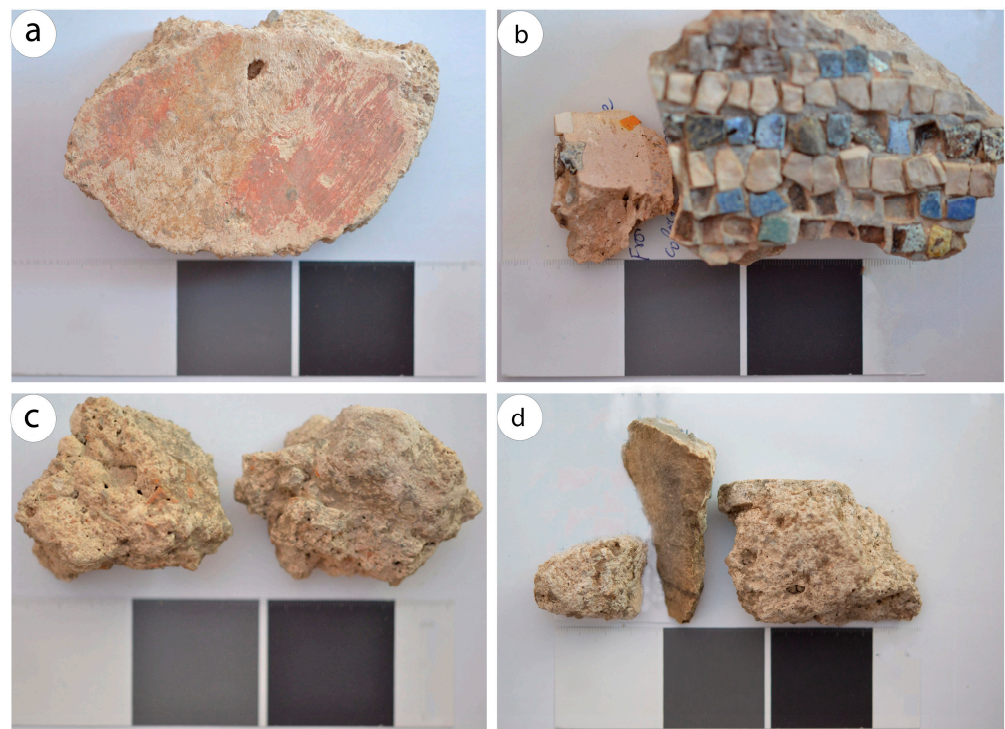


Figure 5. The representative mortar samples; (a) Group 1 (G-1): Painting mortar/render with chromatic layer (samples with stratigraphy); (b) Group 2 (G-2): Preparation mortars with tesserae (samples with stratigraphy); (c) Group 3 (G-3): Filling mortars between marble skirting and wall; (d) Group 4 (G-4): Masonry mortars.

Mortar samples from G-1 and G-2 exhibit stratigraphy. Table 1 summarizes the type of mortars, including information on their characteristics, construction period, function, and location within the *villa*. Macroscopic observations, conducted with the naked eye and a digital camera, reveal the heterogeneity of the mortar samples. The composition includes a light-colored binder and a variety of aggregates differing in color, shape, and size. Lime lumps are prevalent in most of the samples, suggesting incomplete lime extinction, possibly due to insufficient water or time required for lime slaking [20–24].

Painting mortars in G-1 (HT-13P and HT-16P) showcase a reddish chromatic layer over a preparatory/render layer known as *arriccio* (Table 1). These mortars exhibit a disrupted, very thin lime layer (<1 mm), with no observed intermediate layer corresponding to an *intonaco*. Their appearance is heterogeneous, characterized by a gray color and varying sizes and colors of aggregates. Lime lumps and ceramic fragments are also present.

Preparation mortars for wall mosaic tesserae (G-2, HT-20T and HT-22T) display clear stratigraphy with tesserae of different origins/compositions and colors embedded into lime (Table 1). The sequence observed from top to bottom was as follows: (1) tesserae were embedded into a (2) supranucleus, primarily consisting of lime (~1.5–2 cm thick) with rare aggregates of slightly pink/orange color, and a (3) nucleus layer of reddish/orange color with compositionally varied aggregates, including ceramic fragments. This observed stratigraphy aligns with findings from other analytical studies of mosaic preparation [25].

Filling mortars in G-3 (HT-31B and HT-40A), collected from thin and thick walls, respectively, were used to attach marble slabs (skirting) to the walls. They appear light gray and heterogeneous, containing various aggregates (minerals and stones), ceramic fragments, and lime lumps (Table 1).

Table 1. Classification of the mortars from *villa* Horta da Torre based on their function and composition. The stratigraphy of the samples can be compared with the Vitruvian sequence in the Roman mortars: the first layer comprises *tesserae*, followed by the *supranucleus*, *nucleus* (1), and finally the *rudus* or *nucleus* (2) [25,26].

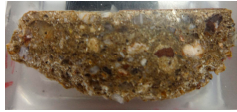

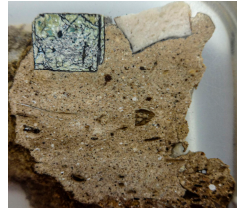

| Group | Sample | Location | Stratigraphy | Description |
|--|--------|---|--|--|
| Group 1 (Painting mortars with chromatic layer) | HT-13P | <i>Peristylum</i> |  | The surface is painted dark red on a white lime base. It is less porous with varying stone aggregate sizes of light gray color. Pieces of terracotta and 'cocciopesto' (crushed ceramics) are also present as aggregate. |
| | HT-16P | <i>Peristylum</i> |  | The top surface is painted red on the thin white lime base. It is less porous with uniform aggregate size (i.e., stones of very light gray in color). |
| Group 2 (Preparative mortars for wall mosaic tesserae) | HT-20T | From Ceiling above the <i>Stibadium</i> |  | Colorful mosaics are embedded into the top surface, and a few pieces are embedded in the mortar bed. The second layer of mortar is compact, light gray in color, and has a lower proportion of aggregate. The third layer is dark gray/brown in color with bigger and more stone aggregates. Other pieces of the sample are thicker and have less porosity but a uniform lime bed. |
| | HT-22T | <i>Triclinium</i> Southwest Wall |  | The top layer of the colorful mosaic is embedded in a hard, light gray lime bed, working as a base for the mosaics. This layer of mortar is compact, porous, and homogenous. The third layer is non-porous with dark gray stone aggregates. |

Table 1. Cont.


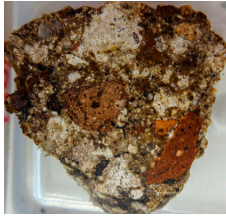
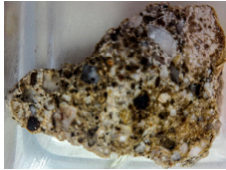



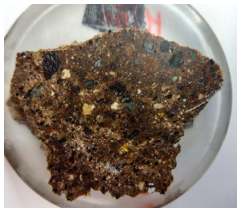
| Group | Sample | Location | Stratigraphy | Description |
|---|--------|----------------------|--|---|
| Group 3 (Filling mortars in between wall and marble cladding) | HT-31B | Narrow Southern Wall |  | It is porous and light gray in color, with big lime lumps present in the mortar. Stone and ceramic/terracotta aggregates of various sizes and shapes are present. |
| | HT-40A | Wider Northern Wall |  | The sample is more porous and lighter gray in color, with a homogenous lime matrix. Stone aggregates of various sizes with some pieces of red ceramics/terracotta are present. It consists of big lime lumps as well. |
| Group 4 (mortars for stone masonry) | HT-18 | Inner Apse |  | The sample is porous and light and dark gray in color. Stone aggregates and lime lumps of various sizes are visible. |
| | HT-19 | Outer Apse |  | It is porous, light gray in color, and has stone aggregates of various sizes. One piece of the sample is a hard stone that is different from the other two samples. The sample contains small lime lumps as well. |

Table 1. Cont.

| Group | Sample | Location | Stratigraphy | Description |
|-------|--------|------------------------|---|---|
| | HT-31A | Narrow Southern Wall |  | It is porous and light gray in color, with lithic aggregates of various sizes and sand particles. |
| | HT-40B | Wider Northern Wall |  | It is less porous and dark gray in color, with a homogenous composition. Stone aggregates of uniform sizes are embedded in the lime matrix. |
| | HT-60 | Wall of the Water Tank |  | It has almost uniform porosity and is dark gray in color, with small lime lumps and stone aggregates of various sizes. It has high compression strength. It looks different from the other samples. |

Lastly, masonry mortars in G-4 (HT-18, HT-19, HT-31A, and HT-40B; Table 1) also exhibit a heterogeneous appearance in terms of material variability and aggregate dimensions. They generally appear light gray, with varying strengths and porosities. One notable sample, HT-60, stands out with its dark gray color, very coarse texture/appearance, consistent lime lumps, and retrogranular aggregates embedded in the matrix.

3.2. X-ray Powder Diffraction

The X-ray powder diffraction (XRD) analysis was conducted on global fractions from the samples of *villa* Horta da Torre. The results are presented in Table 2.

For Group 1 (HT-13P and HT-16P), the analysis revealed the presence of calcite, quartz, feldspars, micas, and clay minerals, with small amounts of amphibole and hematite. The identification of hematite as an inorganic additive suggests its potential role in imparting the reddish color observed in these layers [27]. A representative diffractogram for sample HT-13P is represented in Figure 6a.

In Group 2, corresponding to preparation mortars for wall mosaic tesserae, mineralogical phases in layers enriched with lime (upper layer supporting tesserae HT-20T-2 and HT-22T-2) primarily consist of calcite, with minor occurrences of quartz, K-feldspar, and micas. In contrast, the lower layer (*nucleus*) from sample HT-22T-3 predominantly exhibits calcite associated with K-feldspars, along with quartz, albite, and micas. Figure 6b illustrates the representative diffractogram for sample HT-22.

The filling mortars in Group 3 present calcite as the main phase. However, slight variations in mineralogical phases exist among the samples; in one sample, quartz prevails and is accompanied by some micas, whereas in another sample, feldspars are predominant, associated with less muscovite and quartz. Further details are provided in Table 2 and a representative diffractogram for sample HT-40A is presented in Figure 6c.

In general, Group 4 (masonry mortars) shows minor differences in its mineralogical composition. The results indicate the presence of calcite associated mainly with silicates such as quartz and microcline (Table 2). Additionally, other mineral phases, including phyllosilicates (muscovite, biotite, clinocllore, and clays), amphiboles, and hematite, were also intensified. Figure 6d shows the diffractogram for the global fraction of HT-31A, while the exceptional case of HT-60 stands out due to its different mineralogical composition as previously detected through other techniques. Calcite occurs in small amounts compared to other samples, with quartz and amphibole being the clearly dominant silicates. Micas, albite, and hematite are other phases present in smaller quantities.

3.3. Microscopic Observation

Optical microscopy plays an important role in mortar characterization. This technique facilitates the visualization of microstructures using thin sections, enabling the identification of aggregates and the determination of additives. Moreover, the identification of certain constituents and/or textural aspects aids in interpreting the geological provenance of raw materials [28]. The choice of thin sections primarily focused on those with more complete and well-preserved stratigraphy or samples providing specific and relevant information [29].

The observed sample, HT-13P, typically presents a continuous microcrystalline binder with a red chromatic layer. The overall appearance of this mortar sample reveals granite grains and plagioclase (plg), as demonstrated in Figure 7a,b. Additionally, Figure 8a shows a reddish paint layer on the top, along with calcite binder and quartz. The mortar displays heterogeneity with angular large granitic grains, smaller quartz and plagioclase, alkaline feldspar grains, and rarer biotite and ceramic fragments. A thin and discontinuous preparatory layer is visible, with aggregates occurring at the surface, associated with the red pigment.

Table 2. The mineralogical composition of the global fractions (G.F) for the mortar samples from the *villa* Horta da Torre, Portugal was obtained using XRD analysis.

| Group | Sample | Fraction | Quartz | Calcite | Alkaline Feldspars | Plagioclase | Pyroxene | Micas | Clinocllore | Vermiculite | Amphibole | Hematite | | | |
|--|--------|----------|--------|---------|--------------------|-------------|----------|-------|-------------|-------------|-----------|----------|-------|------|----|
| G-1 (Painting mortar) | HT-13P | G.F | +++++ | + | ++ | +++ | ++ | - | + | +++ | - | - | ± | - | |
| | HT-16P | G.F | +++++ | + | - | ++++ | ++ | - | + | + | + | Tr | - | Tr | |
| G-2 (Preparation mortar for mosaic tesserae from wall) | HT-20T | G.F.2 | + | +++++ | - | + | Tr | - | ± | + | Tr | - | - | - | |
| | HT-22T | G.F.2 | Tr | +++++ | - | + | Tr | - | Tr | Tr | Tr | - | - | - | |
| | | G.F.3 | Tr | +++++ | ± | ++ | Tr | - | + | + | Tr | - | - | - | |
| G-3 (Filling mortar for marble clad) | HT-31B | G.F | ++++ | +++++ | - | + | + | - | Tr | ++ | - | - | tr | - | |
| | HT-40A | G.F | ++ | ++++ | ++ | +++ | ± | - | ± | +++ | Tr | - | Tr | - | |
| G-4 (Masonry mortars for joining stone) | HT-18 | G.F | +++++ | +++ | + | ++++ | ++++ | - | ± | ++ | ± | - | - | - | |
| | HT-19 | G.F | +++++ | +++ | - | ++++ | ++ | - | + | ± | ++ | ± | - | - | Tr |
| | HT-31A | G.F | +++ | ++++ | ++++ | ++++ | ± | - | + | ± | Tr | ± | ±hrn. | ± | |
| | HT-40B | G.F | ++++ | ++ | - | +++++ | ++ | - | Tr | + | Tr | - | Tr | - | |
| | HT-60 | G.F | ++++ | ++ | - | - | ++ | - | Tr Py. | ++ | + | + | - | ++++ | + |

Peak intensity: (+) = abundance ratio of 6; (±) = abundance ratio between 6 and 1 indicating a predominant compound; trace amount (Tr); undetected (-); global fraction (G.F); fine fraction (F.F); Gehlenite (geh.); Epidote (Ep); Hornblende (hrn.); Pyroxene (Py.).

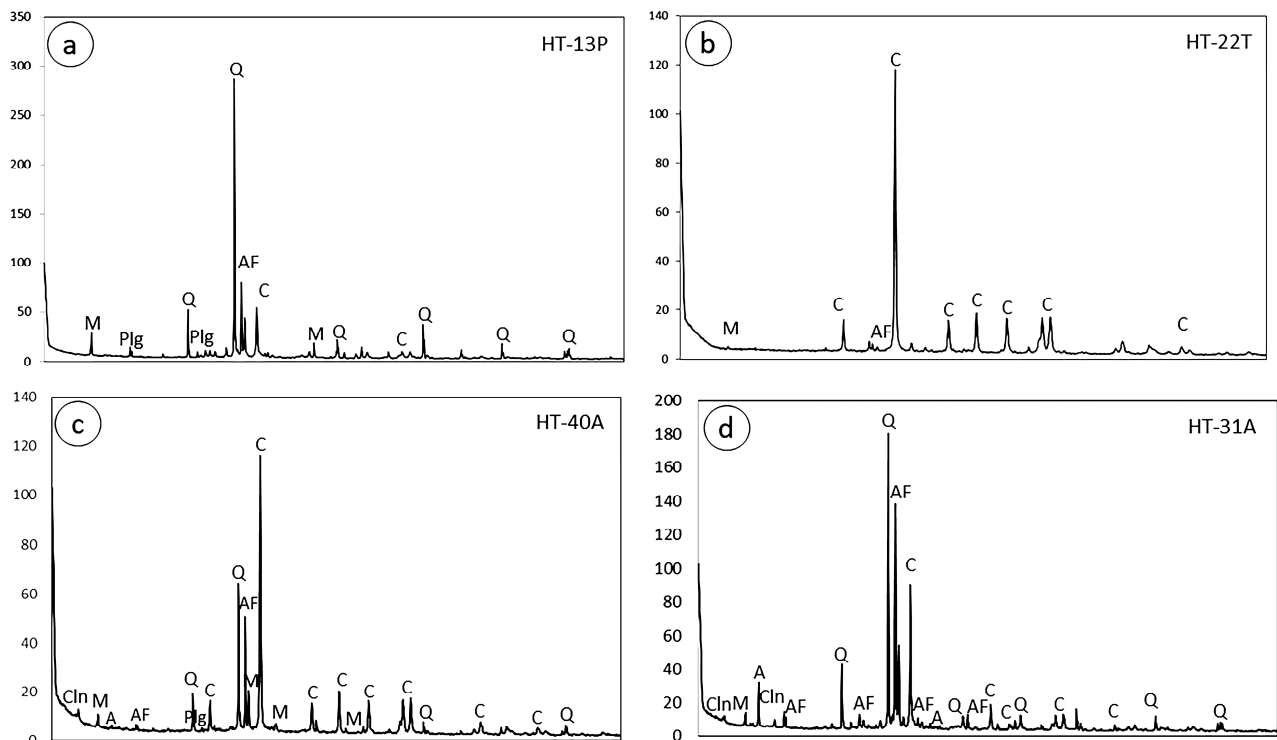


Figure 6. XRD diffractograms obtained for selected samples from *villa* Horta da Torre; (a) HT-13P (quartz, calcite, and feldspars); (b) HT-22 (calcite, quartz, and aragonite); (c) HT-40A (quartz, calcite, and muscovite); (d) HT-31A (calcite, quartz, albite, and orthoclase).

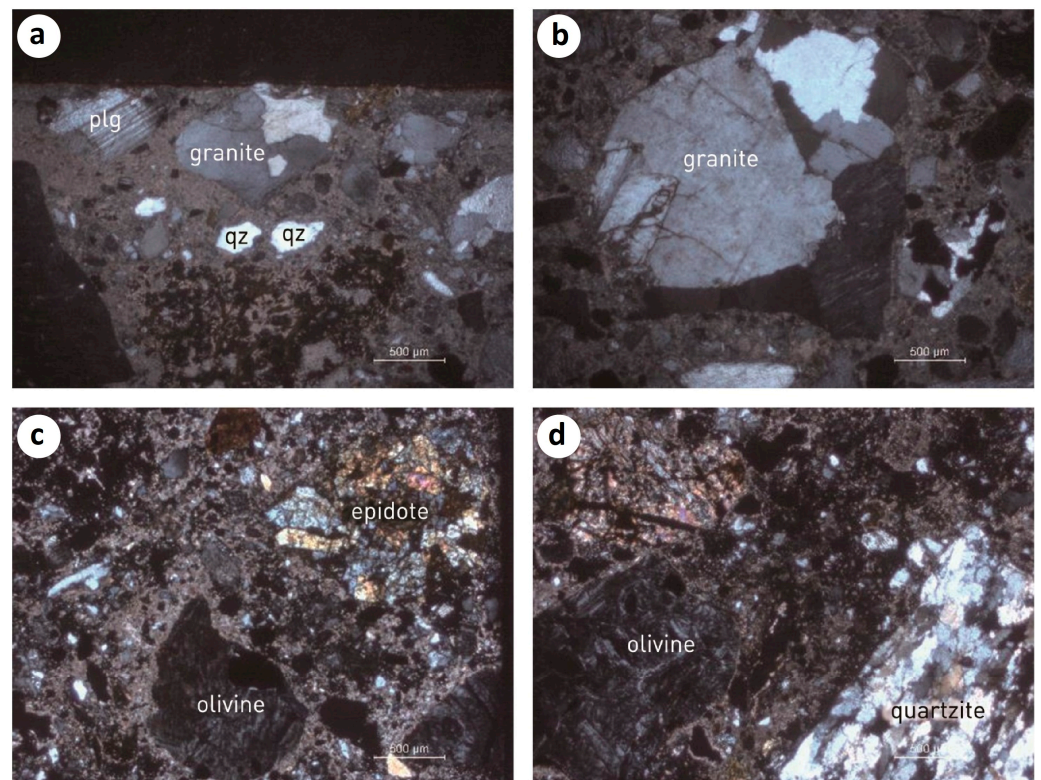


Figure 7. Representative microphotographs of the mortar samples: (a,b) showcase the overall appearance of the mortar in the HT-13P sample, revealing granite grains and plagioclase (plg). In sample HT-60, (c) displays olivine and epidote; (d) exhibits olivine and quartzite.

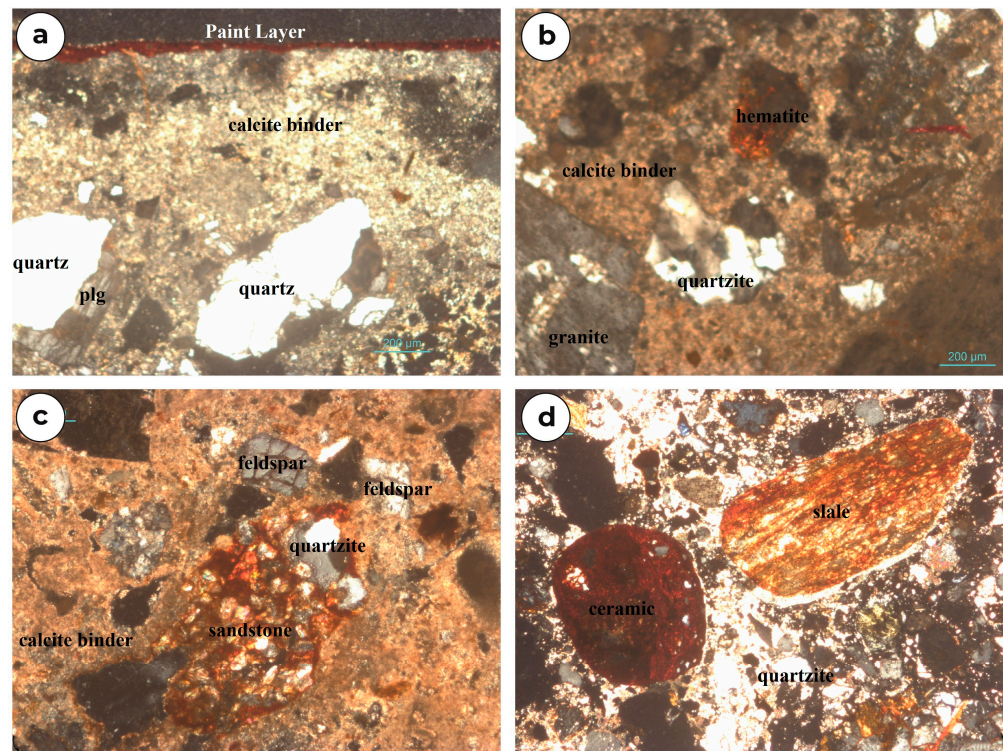


Figure 8. Representative petrographic images of the mortar samples: (a) HT-13P shows a reddish paint layer on the top, calcite binder and quartz; (b) HT-22 reveals calcite binder, hematite, granite, and quartzite in the bottom layer; (c) HT-40A shows quartzite, calcite binder, and feldspar in the mortar bed; (d) HT-60 exhibits ceramic fragments, quartzite, and slale.

Samples from Group 2 (Figure 8b) present similar features. The top layers have microcrystalline granularity and disperse fine particles of clay material. The observed tesserae are composed of glass (green) and limestone (white). The transition between layers is well defined, albeit with an irregular contour at the observed scale. The mortar in the lower layer (*nucleus*) presents a continuous binder with microcrystalline granularity. The aggregates are highly diversified (pyroxene, olivine, plagioclase, alkaline feldspar, ceramic fragments, and quartz) and highly hetero-granular, often presenting angular forms or even crystal faces.

The thin section of sample HT-40A (Figure 8c) from Group 3 mainly comprises quartz and K-feldspar. In addition to ceramics, a wide variety of lithic grains, including metapelite and granitic quartzite, were also observed.

Sample HT-60 from Group 4 presents a heterogeneous microcrystalline binder that envelops an irregular distribution of aggregates. Apparently, there is a decrease in the amount of binder. Aggregates are highly diverse, in a similar way to what was observed in the lower layers of the samples from Group 2 (Figure 7c,d and Figure 8d): olivine (sometimes serpentinized), pyroxene, allanite, oxides, quartzite ceramic fragments, chlorite, amphibole, quartz, and feldspars.

3.4. Acid Attack and Granulometric Analyses

Following stereomicroscopic observations, a specific weighed quantity of each sample fraction underwent careful layer-by-layer disintegration to prevent the breakage of existing aggregates. The disintegrated material was subsequently dried at 40 °C in an oven for 24 h to evaporate the moisture content. The dried sample fraction was then transferred to a beaker, and 120 mL of an aqueous hydrochloric acid solution (HCl; 1:3) was measured separately using a graduated cylinder. The dried samples, initially weighing approximately 10 g (mi), were subjected to (attacked by) the aqueous hydrochloric acid solution. Upon

completion of the chemical reaction, the resulting mixture was heated until ebullition and left for 10 min. This HCl digestion process dissolved the soluble fractions, including calcium carbonate binder, salts, and organic compounds [13], leaving behind an insoluble residue (non-carbonated aggregates).

The insoluble residue was subsequently dried in an oven at 40 °C for 24 h, weighed (mf), and mechanically sieved through a series of standard sieves with mesh sizes of 63 µm, 125 µm, 250 µm, 500 µm, 1 mm, 2 mm, and 4 mm. Microphotographs were taken for each aggregate fraction under the stereo-zoom microscope. The sieved fractions were used to obtain information about particle size distribution and estimate the binder/aggregate ratios within the mortar samples [9,20]. It has been demonstrated that grain size distribution analysis is essential for acquiring information about mortar preparation, specifically regarding constituents and their ratios in the mixture [9]. The results of the acid attack are presented in Table 3, where the insoluble residue mainly comprises siliceous aggregates, with recorded values ranging from 12.47% to 75.69%.

Table 3. Results after acid attack. Grain size distribution (mass %) and classification according to the Wentworth Scale of insoluble residues.

| Sample Name | Insoluble Residue (%) | Grain or Particle Size Distribution of Insoluble Residue/% | | | | | | | |
|-------------|-----------------------|--|----------------------------|----------------------------|-------------------------|----------------------------|----------------------------|---------------------------------|------------------|
| | | >4 mm Fine Gravel | 4–2 mm Very Fine Gravel | 2–1 mm Very Coarse Sand | 1–0.5 mm Coarse Sand | 0.5–0.25 mm Medium Sand | 0.25–0.125 mm Fine Sand | 0.125–0.63 mm Very Fine Sand | <0.63 mm Silt |
| HT-13P | 72.54 | 1.35 | 14.87 | 22.57 | 17.57 | 14.46 | 12.84 | 10.27 | 5.40 |
| HT-16P | 60.70 | 1.36 | 20.75 | 37.66 | 18.91 | 10.26 | 5.69 | 3.44 | 1.20 |
| HT-20T2 | 12.47 | 0 | 0 | 0 | 0 | 19.84 | 40.48 | 31.75 | 6.35 |
| HT-22T2 | 15.71 | 0 | 0 | 0 | 36.65 | 19.88 | 22.36 | 19.26 | 0.62 |
| HT-20T3 | 49.22 | 9.66 | 14.84 | 24.8 | 21.81 | 14.14 | 7.97 | 5.08 | 2.09 |
| HT-22T3 | 55.94 | 4.7 | 17.77 | 21.6 | 18.64 | 15.33 | 10.45 | 7.67 | 1.92 |
| HT-31B | 56.93 | 9.5 | 16.41 | 23.66 | 17.44 | 14.51 | 8.98 | 5.87 | 2.59 |
| HT-40A | 47.13 | 15.13 | 17.86 | 20.17 | 17.65 | 13.45 | 9.24 | 5.25 | 2.10 |
| HT-18 | 64.92 | 7.17 | 25.18 | 32.36 | 18.16 | 9.22 | 4.98 | 2.34 | 0.88 |
| HT-19 | 75.69 | 7.96 | 18.41 | 23.89 | 17.36 | 14.23 | 9.92 | 5.09 | 1.96 |
| HT-31A | 70.48 | 0 | 23.42 | 30.58 | 19.15 | 11.16 | 8.26 | 5.23 | 1.93 |
| HT-40B | 63.81 | 6.49 | 24.65 | 33.54 | 24.57 | 6.03 | 2.55 | 1.46 | 0.70 |
| HT-60 | 72.08 | 17.2 | 11.07 | 12.62 | 14.78 | 13.97 | 14.04 | 11.47 | 5.33 |

After the acid attack, the insoluble residue was sieved. Distribution curves by class are displayed in Figure 9a–d. This granulometric analysis aims to reveal the identical grain size distribution of aggregates among the samples. All types of mortars, including layers within them, display curves with a similar uni-modal shape, with higher values falling in the range of 1 to 2 mm, characterized as coarse sand according to the Wentworth classes of sands (after Wentworth, 1922). The curves tend to be flattened due to the significant contribution of other granulometric fractions (higher and lower grain sizes), validating the heterogeneous appearance. The samples labeled HT-20-3 and HT-22-3 (Figure 9b) correspond to the lower part of the samples, which is the *nucleus*. The HT-60 sample (Figure 9d) shows a different granulometric distribution with a flatter pattern and lacks a clearly defined modal class. The presence of large aggregate fractions (<4 mm to 1 mm) in this sample is attributed to the existence of significant fragments of ceramics.

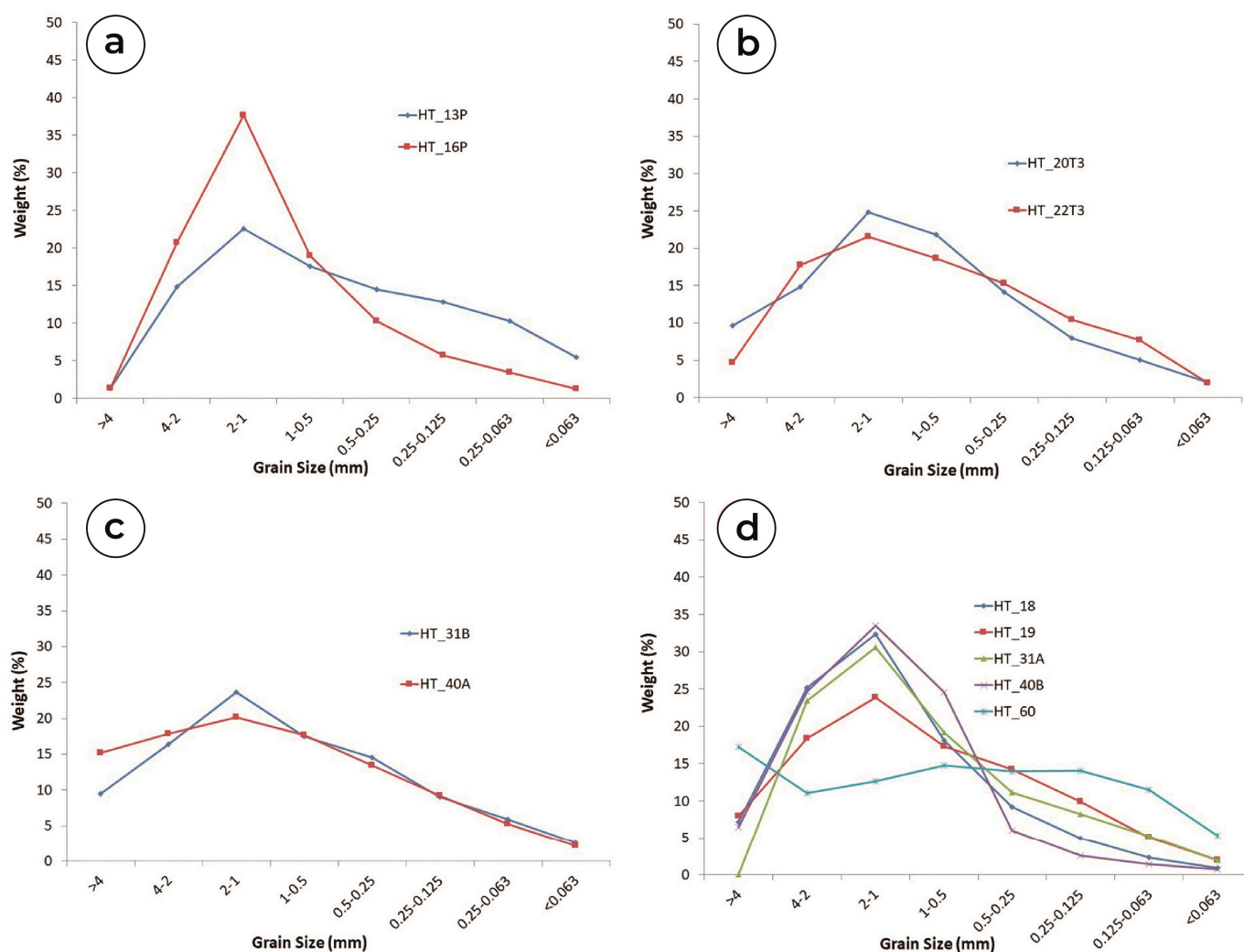


Figure 9. Grain size distribution of the insoluble residues: (a) G–1 painting mortar samples; (b) G–2 mortar samples with tesserae; (c) G–3 filling mortar samples; (d) G–4 masonry mortar samples.

3.5. Thermal Analysis (TGA/DTA)

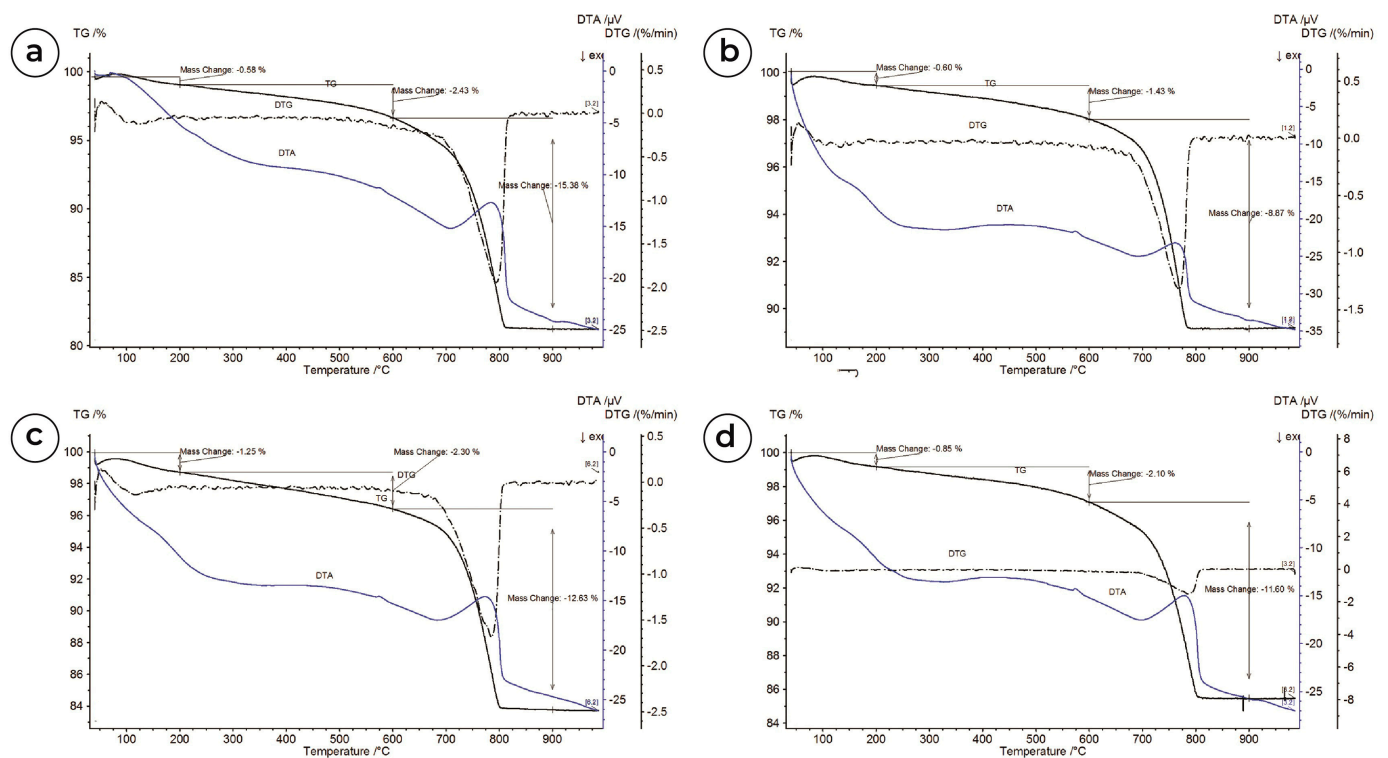
Table 4 and Figure 10a–d present the data obtained from thermogravimetric analyses (TGA) and differential thermal analyses (DTA) conducted on samples from the Roman *villa* of Horta da Torre. The interpretation of the TGA and DTA results enabled us to determine specific weight changes at different temperature intervals.

During the temperature range of 40 °C to 200 °C, the observed weight loss is attributed to the removal of physically adsorbed water [30]. Subsequently, between 120 °C and 200 °C, a decline in weight indicates the loss of crystallized water from hydrated salts [31]. Moving forward, the mass loss recorded between the temperature range of 200–600 °C is attributed to the dihydroxylation of clay minerals [32–34], while the weight loss observed at temperatures between 600 °C and 900 °C is a consequence of CO₂ release due to the decomposition of calcium carbonate CaCO₃ [8,35–39]. Furthermore, a minor peak on the DTA curve at approximately 573 °C is linked to the presence of quartz. This peak results from the transition of quartz- α to quartz- β at that specific temperature [39,40]. These findings provide valuable insights into the thermal behavior of the analyzed samples.

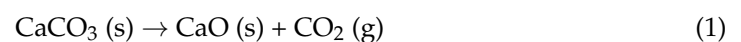
Table 4. TGA weight losses (%), CaCO₃ contents (%), ratio of CO₂/H₂O, and binder-to-aggregate ratios of the mortar samples.

| Group | Sample | Temperature Range (°C) and Weight Loss (%) | | | CaCO ₃ Content | CO ₂ /H ₂ O * | Binder: Aggregate |
|---|----------|--|------------|------------|---------------------------|-------------------------------------|-------------------|
| | | 40–200 °C | 200–600 °C | 600–900 °C | | | |
| G-1 Wall Painting Mortars | HT-13P | 0.6 | 1.43 | 8.87 | 20.2 | 6.20 | 1:4 |
| | HT-16P | 0.93 | 2.45 | 12.69 | 28.9 | 5.18 | 1:2.46 |
| G-2 Preparation Mortars for Wall Tesserae | HT-20T-2 | 2.26 | 3.98 | 31.19 | 70.9 | 7.84 | 1:0.41 |
| | HT-20T-3 | 0.58 | 2.43 | 15.38 | 35.0 | 6.33 | 1:1.86 |
| | HT-22T-2 | 1.59 | 3.87 | 31.08 | 70.7 | 8.03 | 1:0.41 |
| G-3 Filling Mortars for Marble Skirting | HT-31B | 1.25 | 2.30 | 12.63 | 28.7 | 5.49 | 1:2.48 |
| | HT-40A | 1.44 | 3.35 | 20.88 | 47.5 | 6.23 | 1:1.1 |
| G-4 Mortars for Stone Masonry | HT-18 | 0.85 | 2.10 | 11.6 | 26.4 | 5.52 | 1:2.79 |
| | HT-19 | 1.59 | 2.30 | 11.59 | 26.4 | 5.04 | 1:2.79 |
| | HT-31A | 0.38 | 1.85 | 11.82 | 26.9 | 6.38 | 1:2.72 |
| | HT-40B | 0.4 | 2.03 | 14.8 | 33.6 | 7.29 | 1:1.98 |
| | HT-60 | 1.83 | 3.14 | 8.07 | 18.3 | 2.57 | 1:4.46 |

* (percentage weight loss > 600 °C)/(percentage weight loss between 200 °C and 600 °C).

**Figure 10.** Thermograms of the global fraction of samples: (a) HT–20T-1; (b) HT–13P; (c) HT–31B; (d) HT–18 indicating mass losses due to dehydration, hydraulicity, and calcite decomposition.

Thermogravimetric curves for various samples do not show a systematic or clear difference between the four groups of mortars. The most significant mass loss occurs within the temperature range of 600 °C to 900 °C, interpreted as the decomposition of calcite, as shown in Equation (1).



The calculated amount of CaCO₃ varies between 20% and 70%, mainly falling within the range of 20% to 30%. Mass losses in other temperature ranges are less than 4% and

can be attributed primarily to the presence of clay minerals and adsorbed water. The Jedrzejewska method [41] was employed to calculate the simplified composition of mortars. In Equation (2), the soluble fraction represents compounds soluble in acid, 'IR' stands for insoluble residue, and 'carbonates' are calculated from CO₂ loss by TGA. The binder-to-aggregate ratio is calculated according to Equation (2), varying between 2.59% and 16.62% (Table 3) [42,43].

$$\text{Soluble Fraction} = 100 - \sum (\text{IR} + \text{Carbonates}) \quad (2)$$

This ratio ranges from almost pure lime, without a hydraulic component found at G-3, to values denoting significant hydraulicity (*supranucleus* of G-2). Higher values of the soluble fraction are observed in layers of *supranucleus* with a substantial presence of ceramic powder 'cocciopesto' suggesting a potential pozzolanic reaction with lime, leading to the formation of Ca-Al-Si hydrated phases reflected by higher soluble fraction values. The process with lime results in the formation of quasi-gel-like pozzolanic phases, such as C-A-S-H [44]. The observed C-A-S-H phase development in cocciopesto mortars is in agreement with the other studies [45,46]. These phases, commonly observed in pozzolanic products found in ancient cocciopesto-rich mortars, are indicated by the higher soluble fraction values [34].

The CO₂/H₂O ratio has been used as an indicator to evaluate the level of hydraulicity in mortars, as demonstrated by previous studies [35,36,39]. These investigations have unveiled an inverse correlation between the carbon dioxide/structurally bound water ratio and the hydraulic property of a mortar; specifically, a higher ratio is associated with lower hydraulicity, while lower ratios correspond to higher hydraulicity [35,36,39]. However, despite observing similar CO₂/H₂O ratio values across all samples, it is not feasible to conclude that the G-2 samples have greater hydraulicity. The simplified traces for the studied samples were determined (see Table 4). In the *nucleus1* brown mortar, the TGA allows the calculation of an aggregate binder ratio of approximately ~1:2. The soluble fraction indicates a higher ratio of around ~1:1, suggesting the dissolution of organic phases or phases resulting from pozzolanic reactions. Notably, differences are observed in G-3, particularly regarding the binder aggregate ratio (approximately 1:3 for HT-31B and ~1:1 for HT-40A) calculated from TGA results. However, these differences are attenuated in the determination of the soluble fraction. In the case of HT-60, there is again a discrepancy, as the binder aggregate ratio obtained by TGA is low, around 1:5.

3.6. Variable Pressure Scanning Electron Microscopy with Energy Dispersive X-ray Spectroscopy

A variable pressure scanning electron microscope equipped with energy dispersive X-ray spectroscopy (VP-SEM-EDS), operating in a low vacuum system, was used to conduct elemental analysis and determine the composition of aggregates and binders on polished surfaces. The SEM-EDS data not only confirmed and complemented observations made through other techniques but also validated the composition of the binding phase. Both samples of G-1 mortars with paint layer (HT-13P and HT-16P) showed similar texture and elemental composition. Elemental distribution maps and areas analyzed for both samples display calcium (Ca) as the primary element present in the binder. The Figure 11 shows a representative sample, HT-16P. In the analyzed samples, silicon (Si) particles predominantly appeared in the form of quartz, while the association of Si with aluminum (Al) and potassium (K) indicated the presence of K-feldspar, and Al along with Na suggested sodic plagioclase in the aggregates. The preparative layer consisted primarily of Ca-rich aerial lime. The transition from the preparative layer to the lower mortar was marked by a slight increase in Mg and Al (Figure 11a–f).

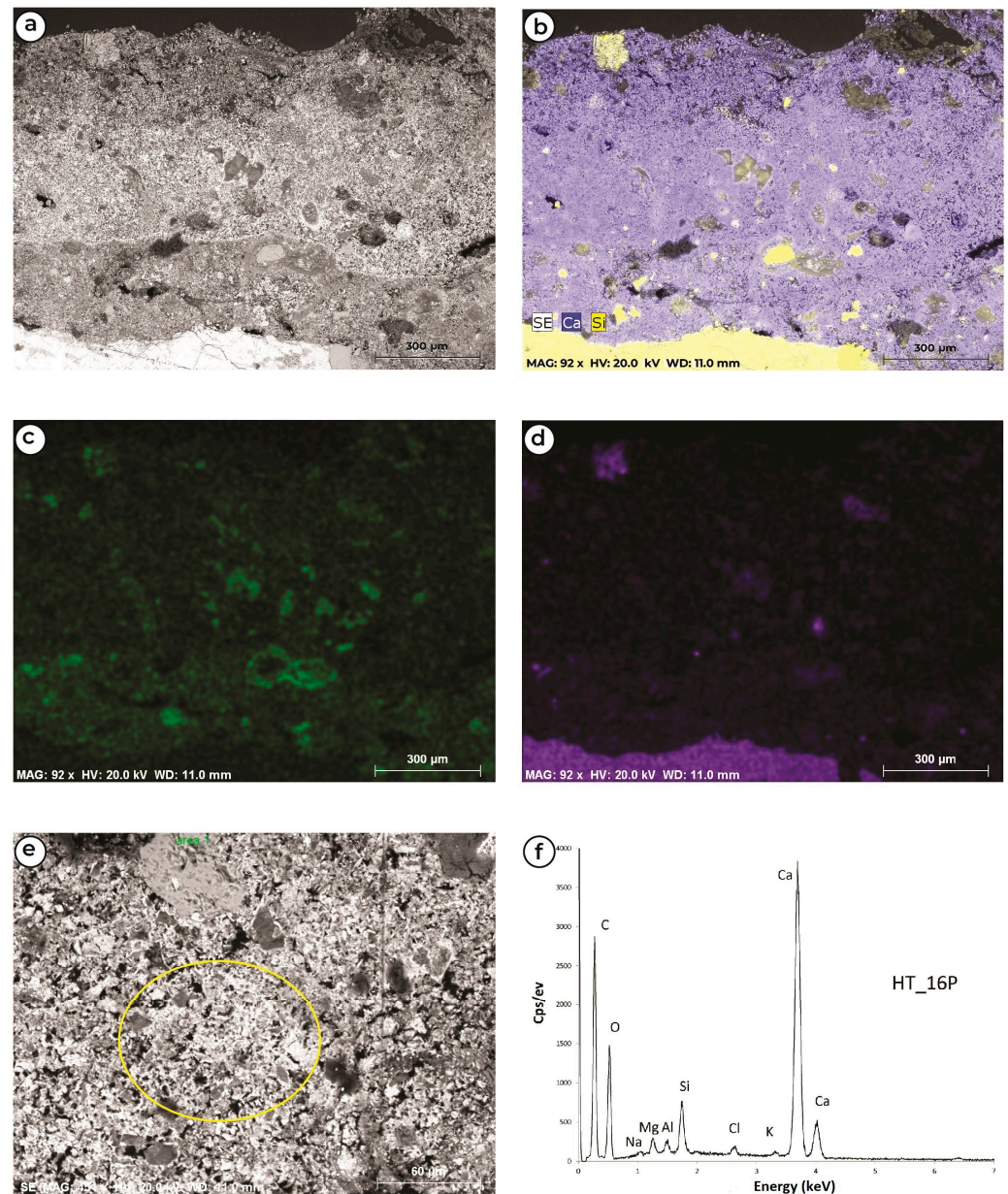


Figure 11. HT-16P: (a) BSE image showing the transition between preparative layer and mortar; (b) BSE and EDS elemental distribution map for Ca and Si; (c) EDS elemental distribution map for Mg; (d) EDS elemental distribution map for Al; (e) BSE image showing of the preparative layer texture; (f) the corresponding EDS spectrum is presented in the yellow-circled area depicted in (e). Samples from G-2 (HT-20T and HT-22T) exhibit a top layer, known as the *supranucleus*, primarily composed of calcitic lime (Ca), as shown in Figure 12, featuring a homogeneous and continuous texture. This layer also incorporates fine ceramic powder (K, Al), contributing to an orange hue, as illustrated in Figure 12e. The underlying mortar layer reveals aggregates of quartz (Si), alkali feldspar (K, Si, Al), pyroxene (Fe, Mg, Si), olivine (Mg), and ceramic fragments (Al, Fe, Mg, K) as depicted in Figure 12.

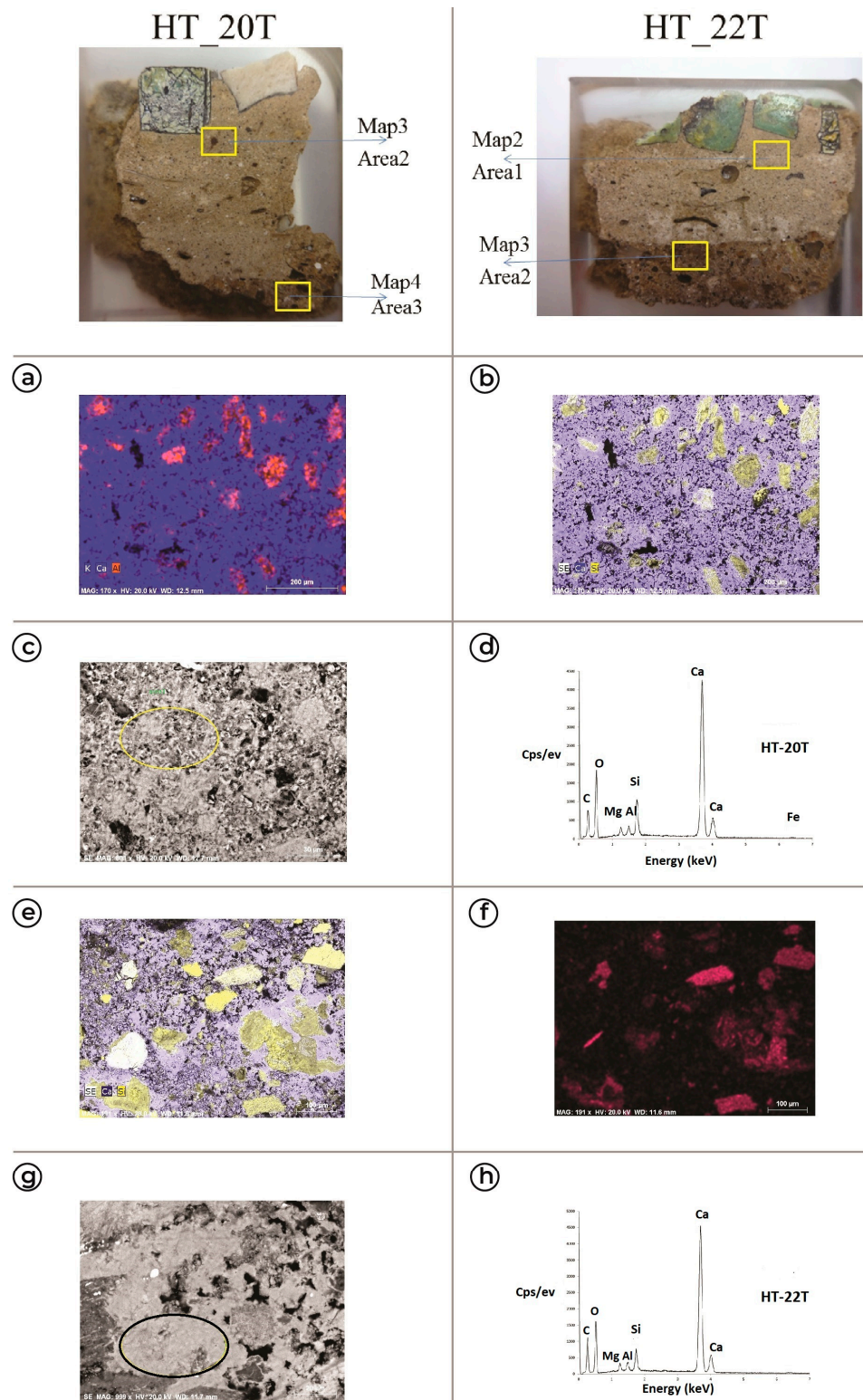


Figure 12. Samples with tesserae HT-20T (a–d) and HT-22T (e–h): (a) EDS elemental distribution map for Ca and Al in the top layer from HT-20T; (b) BSE and EDS elemental distribution map for Ca and Si; (c) BSE image of microstructure of the binder matrix; (d) the corresponding EDS spectrum on the area highlighted in the image; (e) BSE and EDS elemental distribution map for Ca and Si for the HT-22T lower layer; (f) EDS elemental distribution map for Al; (g) BSE image of microstructure of the binder matrix; (h) the corresponding EDS spectrum on the area highlighted in (g).

In both layers, in addition to calcium, the binder also contains elements such as Si, Al, and Mg, which is evident from Figure 12 (spectra d and h). The presence of these elements, particularly Al, Si, and Mg, in the binder phase might be associated with the presence of clay minerals. These minerals might originate from the fine component or the clay components present in the raw material (marly limestone) consumed for the production of lime. Since the pozzolanic reactions are neither evident nor identified with XRD analysis, it is plausible to suggest that the binder is primarily related to the development of M-(A)-S-H phases rather than marly limestone. Furthermore, the presence of dolostones or crestline limestones might reinforce this presumption.

Figure 13 presents elemental distribution maps derived from BSE and EDS analyses. Subfigure (a) shows the distribution of Ca, K, and Si, while (e) displays the EDS spectrum of sample HT-13P, indicating its elemental composition as Ca, Si, Al, Na, K, and Mg. Sample HT-18 is represented in (b), indicating quartz, k-feldspar, and ceramics in its top layer, with (f) displaying its elemental distribution. Subfigures (c) and (d) analyze the lower layer of the sample HT-60, and provide elemental distribution across the sample.

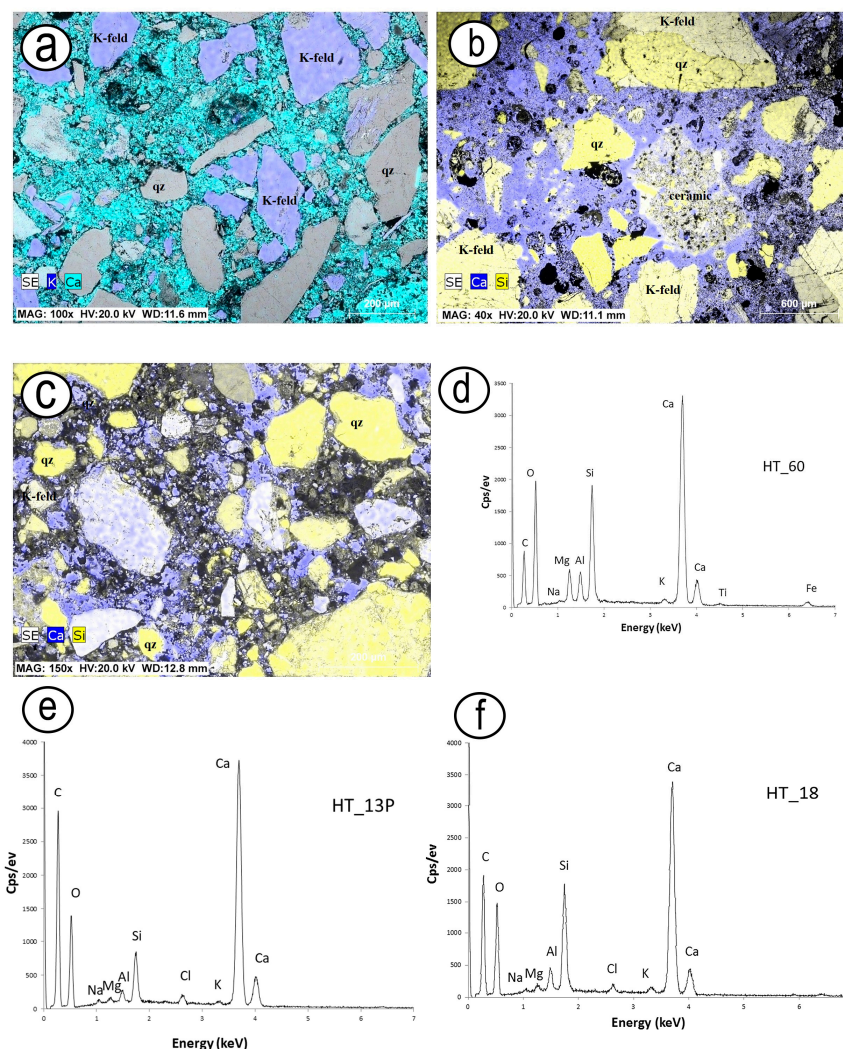


Figure 13. (a) BSE and EDS elemental distribution map for Ca and K or Si for the sample HT-13P; (b) BSE and EDS elemental distribution map for Ca and Si in the top layer from HT-18; (c) BSE and EDS elemental distribution map for Ca and Si for the HT-60; (d) an elemental distribution of HT-60; (e) the EDS spectrum of HT-13P; (f) an elemental distribution of HT-18. The aggregates, identified through microscopy, XRD, and SEM-EDS, exhibit marked distinctions (quartz, potassium feldspar,

pyroxene, olivine, ceramic fragments), indicating a significant geological variability in the source of the sand material. The filling mortars in the studied samples from G-3 have a more discontinuous binder texture, yet they present similar features regarding binder and aggregate composition. Despite the same application context of the mortars, the results obtained seem to indicate some differences in production techniques, which may be related to the type of wall and its structural function in the building.

The representative filling mortar sample HT-31B from G-3 is presented in Figure 14a, which highlights the mapping and binder area analyzed. The samples HT-31B and HT-40A exhibit a more discontinuous binder texture and analysis of their elemental distribution maps (Figure 14b,c). The area examined (Figure 14d, yellow highlighted area) indicates calcium (Ca) as the primary element present in the binder. Silicon (Si) particles are predominantly observed as quartz, while the presence of Si alongside aluminum (Al) and potassium (K) suggests the presence of K-feldspar, and Al along with Na suggested sodic plagioclase in the aggregates (Figure 14e). The higher concentration of Si, Al, Mg, and Na suggests the development of M-S-H or M-(A)-S-H phases [25]. Therefore, the G-3 mortars share similar characteristics regarding binder and aggregate compositions. However, despite being applied in similar contexts, the results suggest potential differences in production techniques, which may be related to the type of wall and its structural function within the building.

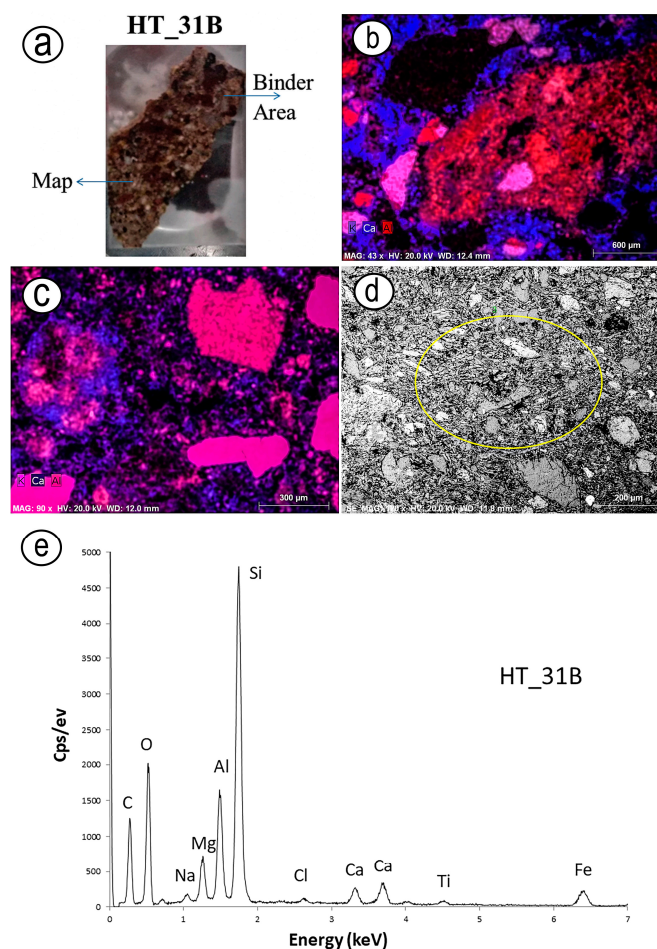


Figure 14. Filling mortar samples from G-3: (a) photograph showing the mapping and binder area analyzed for sample HT-31B; (b,c) representative EDS elemental distribution map for Ca and Al from HT-31B and HT-40A respectively; (d) BSE image of microstructure of the binder matrix for the sample HT-31B; (e) the corresponding EDS spectrum for the yellow-circled area is highlighted in the image (d).

Considering the masonry mortar G-4 samples, specifically HT-18 and HT-19 obtained from the double apse structure, only marginal differences were observed. The binder in HT-18 presents a textural continuity, with the predominant aggregates consisting mainly of quartz (Si in Figure 13b), and quartz, K-feldspar, and occasional fragments of ceramics (Figure 13b). Some of the larger grains show multi-mineral composition and correspond to granitic aggregates. The presence of these aggregates, associated with a considerable amount of feldspars showing a general angular form, suggests a limited transportation distance from the geological source. In sample HT-13P, the composition of the binder is mainly enriched in Ca (Figure 13a), indicating an aerial calcitic lime. However, HT-19 exhibits a higher concentration of silicates, probably clay material. The higher concentration of Si, Al, Mg, and Na suggests the development of M-S-H or M-(A)-S-H phases [27], which are structurally similar to smectite clays. It is imperative to recognize these phases not as intrusions of clay but as resultant products within the binder matrix.

The HT-60 mortar sample is associated with the small water tank beside the *triclimum*. This mortar is distinguished from other samples by significant heterogeneity in both aggregates and their dimensional variability (Figure 13c). The aggregates include quartz, feldspar, granites, olivine (partially serpentinized), pyroxene, quartzite, epidote, and ceramic fragments, all presenting highly angular shapes. The binder content is reduced and irregularly distributed, appearing more discontinuous. While predominantly rich in calcium, it also contains elements such as Al, Si, and Mg (Figure 13d). In this way, the raw material used in this lime mortar appears to share similarities with that employed in other mortar compositions.

4. Discussion

The samples collected from *villa* Horta da Torre in Portugal were categorized into four groups based on their function within the building complex. Variations in their composition were attributed theoretically to mortar function, structural differences, the period of construction/production, and potential sampling limitations. Despite the differences in analytical techniques utilized, similarities and differences between the various mortar types were observed, indicating intentionality in the production of specific mortar types.

4.1. Production Technology

Determining the binder-to-aggregate ratios using TGA and acid attack revealed significant variability ranging from 1:1 to 1:4, with no clear correlation to different mortar types. Although 1:2 ratios predominated, the observed variability may reflect the heterogeneity of the samples. Nevertheless, intentional preparation was observed in some mortars/layers, such as the consistent lime amount for the *supranucleus* layer (G-2). Besides HT-60, the sand grain size was uniform for all types of mortars, including render and filling or masonry mortars.

Mortars/Render with Painted Surfaces (G-1): These mortar samples showed that the preparative lime layer was thin, discontinuous, and unevenly applied. Very coarse sand aggregates were exposed in the top chromatic layer, with binder-to-aggregate ratios of ~1:3 and ~1:4, along with the same kind of angular aggregate fractions and ceramics in varying proportions. For these mortars (mortars with the chromatic layer), it should be noted that the variability of minerals (e.g., iron–magnesium minerals such as olivine or pyroxene) and lithologies (metamorphic) was not verified as in other samples. In fact, the type of aggregates found agrees with a granitic source. The selection of this material may result from a more refined application, such as mortars that support wall paintings. However, the lime layer is either exceedingly thin or nonexistent, and the aggregates can even outcrop at the surface. Indeed, there is a very fine and discontinuous layer of lime that would regularize the surface. However, the level of crushed marble layer (*intonaco* or *intonachino*) referred to by Vitruvius is absent. This layer typically consists of marble dust as fine-grained aggregates or, more frequently, spray calcite [47]. The use of a very fine ‘*intonaco*’ layer devoid of calcite is mentioned in literature related to late antiquity [48].

Regarding composition, the aggregates present in the *intonaco* layer of mural paintings generally comprise fine-grained sand or crushed marble combined with lime [49,50].

Preparative Mortars with Mosaic *Tessellae* (G-2): The samples of preparative mortar layers of wall mosaic *tessellae* comprised three stratigraphic layers. The *supranucleus* (supports the *tesserae*) was homogenous, primarily composed (~70%) of calcite, with very small ceramic grains (powder). Quartz, feldspar, and ceramics were the main constituents of *nucleus1*, in all the samples, with a binder-to-aggregate ratio of ~1:2. It contains very coarse sand that resembles masonry mortar aggregates.

Filling Mortars (G-3): The samples have the same application context but showed different aggregate minerals and binder-to-aggregate ratios of ~1:1 and ~1:3. The differences may lead to the assumption that they have different production techniques that could be related to different wall types and their varying structural function.

The different groups studied show some internal discrepancies, particularly with respect to the calculation of the trace. Different ratios may reflect a lack of representativeness or a different chronology. There are differences between the functional groups, reflecting an intentionality in the preparation of the different mortars, namely by the addition of ceramics. However, especially regarding the mural paintings, there was not much precept in the finalization.

For the samples HT-31B and HT-40A from Group 3, only slight differences are recorded between the natures of the sand. Therefore, the construction might not be related to two distinct construction episodes. However, the locations of the walls have more influence as the grain size of sand remains the same. The identical grain size distribution of aggregates between the samples indicates a similar picking procedure; the sand seems to be sieved at a cut of around 3–4 mm without a clear differentiation for each type of use. The significant contribution of the remaining granulometric fractions contributes to the heterogeneous appearance of mortars.

Masonry Mortars (G-4): These mortars displayed varying results within the group, with different binder-to-aggregate ratios of ~1:2, ~1:3, and ~1:5. They exhibited a variety of grain sizes in general and very coarse sand in particular, giving them coarser appearance. The sample HT-60, associated with the water tank, showed different results from other samples; this may be due to its distinct functional application.

The mortar samples HT-18 and HT-19 (Group 4) hold particular significance as they originated from the double apses structure, a unique architectural feature in the Portuguese territory. Also, from a textural perspective, the binder in sample HT-18 is more continuous, contrasting with a greater discontinuity observed in the mortar of sample HT-19. In particular, these masonry samples (HT-18 and HT-19) are associated with the double apse structure. According to Carneiro, A. [51], the outer apse (HT-19) is believed to belong to the foundation period, while the inner apse (HT-18) was added later. Despite this chronological distinction, no major differences were identified in the binder proportion (1:3), composition, or the aggregates used. Hence, this similarity suggests a common origin (provenance) for the lime raw material, and thus does not confirm distinct construction episodes.

Sample HT-60 (G-4) was collected from an inside wall associated with a water tank. It visually stands out for its dark gray color, compactness, lime lumps, well-defined porosity, and varied aggregates in size and composition with angular shapes. The binder phase appeared reduced and irregularly distributed. SEM-EDS analyses align with XRD evaluation regarding the main aggregate minerals but also reveal the possible occurrence of quartz and feldspars associated with lithic granitic grains. Additionally, the analyses exposed angular forms of silicates and lithic grains. The compositional variability of the aggregates, detected by optical microscopy and SEM-EDS, includes high proportions of quartz, feldspars, pyroxene, olivine, multi-grained olivine, quartzite, epidote, granites, metapelites, and ceramics, (Figure 7c,d). Conversely, its granulometric distribution curve differs significantly from others (Figure 9d) due to a comparable amount of various granulometric classes. Moreover, it is noteworthy that this mortar exhibits the smallest amount of analyzed calcite as a binder, as determined by both TGA and OM. The uniqueness of this sample lies in its association

with the wall of a structure designed to accumulate water, serving a specific function distinct from most of the other samples. In the Roman era, mortars rich in cocciopesto, prevalent in environments characterized by high humidity or direct water exposure, such as flooring, baths, and cisterns, attracted particular scholarly interest due to their effectiveness in discerning structural applications [50].

4.2. Raw Materials and Provenance

Regarding the nature of sand used as aggregates, XRD analysis revealed no major differences for most samples. The results indicated that the majority of samples predominantly consisted of quartz and feldspars as major aggregates, associated with small or trace amounts of clay minerals, biotite, muscovite, amphiboles, and hematite. These findings were consistent with observations from optical microscopy and SEM-EDS, which additionally highlighted the presence of ceramic fragments, granitic aggregates (observed in HT-13P and HT-16P), and the preservation of crystal faces of some K-feldspar and plagioclase. The prevalence of feldspars, combined with the generally angular shape of the aggregates (sometimes prismatic feldspars) and granitic grains, suggests a locally sourced origin with minimal or no transportation from a nearby source, likely a gravel pit. For the majority of the samples, these aggregates are consistent with a granitic occurrence. This lithology outcrops to the southwest of the *villa* within a distance of less than 3 km.

Nevertheless, it is essential to highlight the HT-60 (G-4) sample and the *nucleus 1* from the G-2 samples. These samples showed, in addition to the abundant presence of quartz observed through OM and SEM-EDS, a minimal amount of feldspar accompanied by iron–magnesium minerals such as pyroxene, epidote, and olivine. The materials found in HT-60 and the base of HT-22 and HT-20 once again suggest a local provenance of sands without associated transportation but are geologically incompatible with a unique granitic source mentioned earlier. The preservation of olivine and pyroxene crystals (Fe and Mg silicates) in these mortars indicates a very local provenance from the igneous mafic massif geological source. This is in accordance with the geological context occurring within a distance of less than 2–3 km (Alter de Chão ultrabasic intrusion). This distinction in provenance aligns with the geological context, where materials to the south are granitic, and those further north are metamorphic or associated with the Alter de Chão ultrabasic intrusion. This appears to be in agreement with two sand exploration sites, gravel pits, or river sands with minimal transportation. Some mortars show a mixture of these two types of sands.

The identification of calcite is interpreted as the main constituent of the binder, with its calcitic aerial nature and lower Si, Al, and Mg content, was consistent with other analyzed binders. The observed elevation in Al and Mg levels within the binder matrix may be attributed to the presence of phyllosilicates and the subsequent formation of M-S-H or M-(A)-S-H phases [52–54] through pozzolanic reactions. Existing literature on ancient and modern mortars confirms the frequent presence of para-pozzolanic phases, characterized by a low-crystalline quasi-phyllosilicate mineral structure [55].

Regarding the provenance of lime, in the vicinity of *villa* Horta da Torre, there is a geological unit of crystalline limestone and dolomites from the lower Cambrian where calcite and dolomite occur in varying proportions. The composition of lime appears to result from the calcination of the same type of essentially limestone raw material (with a small amount of Mg) in various applications studied. This carbonate unit would be volumetrically feasible and recognizable, considering its potential exploration as an ornamental stone in modern times [56]. In the context of volumetric feasibility and recognition of this carbonate unit, particularly when assessing its potential utilization as an ornamental stone in contemporary applications, it is crucial to reassess the association between Mg and Mg-rich limes considering the observed M-S-H or M-(A)-S-H phases [27,51,55].

5. Conclusions

The objective of this research was to characterize various mortar types, investigate their manufacturing technology, and propose the geological provenance of their raw mate-

rials. The mortar samples were systematically categorized into four groups based on their functional roles within the *villa*. In all samples, the binder used was calcitic aerial lime obtained through the calcination of crystalline limestone, with a rare dolomitic component likely sourced from the vicinity of the *villa*. Regarding aggregates, the presence of lithic grains (coarse-grained rocks) and preserved prismatic shapes suggested minimal to negligible transportation from their geological source. Specifically, the aggregates appeared to have been sourced from either river sand or a nearby gravel pit. While the aggregates exhibited some diversity, they consistently aligned with the local geological provenance within a distance of less than 3 km. This finding is also in accordance with the evidence from two sand exploration sites.

Despite exhibiting refined taste and aesthetic peculiarities, it seems that minimal attention was paid to the preparation of different mortars. The sands appeared coarser than those typically found in other contemporary Roman *villae* [57]. Furthermore, they lacked distinctions in their usage and displayed uniform granularity regardless of application type. The selection of raw materials and manufacturing techniques may lead to the assumption that the *villa* was situated approximately 300 km away from the Roman governing center in Hispania. Therefore, it is plausible that the builders either did not deliberately select the construction materials or were constrained by their socio-economic circumstances, unable to afford finer alternative materials.

Author Contributions: Conceptualization, A.D., A.C., C.G. and P.M.; methodology, A.D., P.M. and C.G.; software, A.D., P.M. and C.G.; validation, A.D., A.C., C.G. and P.M.; formal analysis, A.D., P.M. and C.G.; investigation, A.D., P.M. and C.G.; resources, P.M., C.G. and A.C.; data curation, A.D., P.M. and C.G.; writing—original draft preparation, A.D.; writing—review and editing, P.M. and C.G.; visualization, A.D.; supervision, P.M. and C.G.; project administration, P.M. and C.G.; funding acquisition; A.D., P.M., C.G. and A.C. All authors have read and agreed to the published version of the manuscript.

Funding: This project has received funding from the European Union’s Horizon 2020 research and innovation program with agreement number 2018-1468/001-001 and project number 599247-EPP-1-2018-1-PT-EPPKA1-JMD-MOB.

Data Availability Statement: The extended data was submitted in the form of a thesis to the repository of the University of Évora, Évora, Portugal. The presented data is available from the corresponding author upon reasonable request.

Acknowledgments: The authors acknowledge the financial support of ARCHMAT Erasmus Mundus project (the corresponding author was an EACEA Scholarship Recipient) and the cooperation of the Municipality of Fronteira, Portugal. We recognize the sincere support of Director Centro HERCULES Laboratories for providing unconditional technical provision and access to the laboratory equipment. We also wish to thank Massimo Beltrame, Jorge Velez, Luís Dias, and Sandra Velez from the University of Évora, Portugal, and Eisha Imran, Muhammad Umer, and Yaru Meng from Southeast University Nanjing, China. The authors wish to acknowledge “Laboratório HERCULES—Herança Cultural, Estudos e Salvaguarda” funded by FCT—Fundação para Ciência e a Tecnologia, I. P. under reference UIDB/04449/2020, (DOI 10.54499/UIDB/04449/2020) and “IN2PAST—Associate Laboratory for Research and Innovation in Heritage, Arts, Sustainability and Territory” funded by FCT—Fundação para Ciência e a Tecnologia, I. P. under reference LA/P/0132/2020 (DOI 10.54499/LA/P/0132/2020).

Conflicts of Interest: The authors declare that we do not have competing interests to influence the research presented in this article. “The authors declare no conflicts of interest.” This work was originally produced during the ARCHMAT Erasmus Mundus master’s thesis project. “The funders had no role in the design of the study; in the collection, analyses, or interpretation of data; in the writing of the manuscript; or in the decision to publish the results”.

References

1. Artioli, G.; Secco, M.; Addis, A. The Vitruvian legacy: Mortars and binders before and after the Roman world. In *EMU Notes Mineralogy*; Mineralogical Society of Great Britain and Ireland: London, UK, 2019; Volume 20, pp. 151–202. [[CrossRef](#)]
2. Lancaster, L.C. Mortars and plasters—How mortars were made. The literary sources. *Archaeol. Anthropol. Sci.* **2021**, *13*, 192. [[CrossRef](#)]

3. Torraca, G. *Lectures on Materials Science for Architectural Conservation*; Getty Institute: Los Angeles, CA, USA, 2009.
4. Lugli, G. *La Tecnica Edilizia Romana: Con Particolare Riguardo a Roma e Lazio*; G. Bardì: Firenze, Italy, 1957.
5. Ventolà, L.; Vendrell, M.; Giraldez, P.; Merino, L. Traditional organic additives improve lime mortars: New old 20 materials for restoration and building natural stone fabrics. *Constr. Build. Mater.* **2011**, *25*, 3313–3318. [[CrossRef](#)]
6. Von Landsberg, D. History of quicklime production and use from early times to the industrial revolution. *ZKG Int. Ed. B* **1992**, *45*, 269–273.
7. Curulli, A.; Montesperelli, G.; Ronca, S.; Cavalagli, N.; Ubertini, F.; Padeletti, G.; Vecchio Cipriotti, S. A multidisciplinary approach to the mortars characterization from the Town Walls of Gubbio (Perugia, Italy). *J. Therm. Anal. Calorim.* **2020**, *142*, 1721–1737. [[CrossRef](#)]
8. Moropoulou, A.; Bakolas, A.; Bisbikou, K. Investigation of the technology of historic mortars. *J. Cult. Herit.* **2000**, *1*, 45–58. [[CrossRef](#)]
9. Rua, H. *The Ten Books on Architecture by Vitruvius*; IST: Lisbon, Portugal, 1998.
10. Hobbs, L.W.; Siddall, R. Cementitious materials of the ancient world. In *Building Roma Aeterna: Current Research on Roman Mortar and Concrete, Proceedings of the Conference, Helsinki, Finland, 27–29 March 2008*; Ringbom, Å., Hohlfelder, R.L., Eds.; Commentationes Humanarum Litterarum; Societas Scientiarum Fennica: Helsinki, Finland, 2011; Volume 128, pp. 34–58.
11. Ergenç, D.; Fort, R. Multi-technical characterization of Roman mortars from Complutum, Spain. *Measurement* **2019**, *147*, 106876. [[CrossRef](#)]
12. Silva, A.S.; Adriano, P.; Magalhães, A.; Pires, J.; Carvalho, A.; Cruz, A.J.; Candeias, A. Characterization of historical mortars from Alentejo's religious buildings. *Int. J. Archit. Herit.* **2010**, *4*, 138–154. [[CrossRef](#)]
13. Esposito, D.; Conte, A.M.; Corda, L.; Giorgi, E. An interdisciplinary approach for the historical and technical characterization of medieval and modern mortars. *Conserv. Sci. Cult. Herit.* **2020**, *20*, 197–212.
14. Carneiro, A. Adapting to change in rural Lusitania: Zooarchaeological records in the Horta da Torre Roman villa (Portugal). *Eur. J. Post Class. Archaeol.* **2020**, *10*, 247–278.
15. Edmondson, J. A Tale of Two Colonies: Augusta Emerita (Mérida) and Metellinum (Medellín) in Roman Lusitania. In *Roman Colonies in the First Century of their Foundation*; Torrossa Online Digital Bookstore: Oxford, UK, 2011; pp. 32–54.
16. Myers, P.J. Developing Identities within Roman Iberia: Hybridity, Urbanism, and Economics in Southern Iberia in the Second and First Centuries BC. Doctoral Dissertation, University of Birmingham: Birmingham, UK, 2016.
17. Oliveira, R.J.; Neves, S.; Caldeira, B.; Borges, J.F.; Teixidó, T. Desenvolvimento de Metodologias eficazes de Prospecção Geofísica Aplicadas a diferentes Ambientes Arqueológicos: O Caso de Horta da Torre (resultados preliminares). In *Workshop de Ciências da Terra e do Espaço*; Universidade de Évora: Évora, Portugal, 2015. [[CrossRef](#)]
18. Carneiro, A. *O Final Das Villae na Lusitânia Romana. O Exemplo da Horta da Torre (Fronteira)*; URBS REGIA: Toledo, Spain, 2017.
19. Carneiro, A. *Lugares, Tempos e Pessoas. Povoamento Rural Romano no Alto Alentejo*; Humanitas Supplementum no; Imprensa da Universidade de Coimbra: Coimbra, Portugal, 2014.
20. Cardoso, I.; Macedo, M.F.; Vermeulen, F.; Corsi, C.; Santos Silva, A.; Rosado, L.; Mirao, J. A Multidisciplinary Approach to the Study of Archaeological Mortars from the Town of Ammaia in the Roman Province of Lusitania (Portugal). *Archaeometry* **2014**, *56*, 1–24. [[CrossRef](#)]
21. Velosa, A.L.; Coroado, J.; Veiga MD, R.; Rocha, F. Characterisation of Roman mortars from Conímbriga with respects to their repair. *Mater. Charact.* **2007**, *58*, 1208–1216. [[CrossRef](#)]
22. Callebaut, K.; Elsen, J.; Van Balen, K.; Viaene, W. Nineteenth century hydraulic restoration mortars in the Saint Michael's Church (Leuven, Belgium): Natural hydraulic lime or cement? *Cem. Concr. Res.* **2001**, *31*, 397–403. [[CrossRef](#)]
23. Paiva, H.; Silva, L.M.; Labrincha, J.A.; Ferreira, V.M. Effects of a water-retaining agent on the rheological behavior of a single-coat render mortar. *Cem. Concr. Res.* **2006**, *36*, 1257–1262. [[CrossRef](#)]
24. Grilo, J.; Faria, P.; Veiga, R.; Silva, A.S.; Silva, V.; Velosa, A. New natural hydraulic lime mortars—physical and microstructural properties in different curing conditions. *Constr. Build. Mater.* **2014**, *54*, 378–384. [[CrossRef](#)]
25. Secco, M.; Dilaria, S.; Addis, A.; Bonetto, J.; Artioli, G.; Salvadori, M. The Evolution of the Vitruvian Recipes over 500 Years of Floor-Making Techniques: The Case Studies of the Domus delle Bestie Ferite and the Domus di Tito Macro (Aquileia, Italy). *Archaeometry* **2018**, *60*, 185–206. [[CrossRef](#)]
26. Moore, R.E. A newly observed stratum in Roman floor mosaics. *Am. J. Archaeol.* **1968**, *72*, 57–68. [[CrossRef](#)]
27. Ponce-Antón, G.; Zuluaga, M.C.; Ortega, L.A.; Agirre Mauleon, J. Petrographic and chemical–mineralogical characterization of mortars from the cistern at Amaiur castle (Navarre, Spain). *Minerals* **2020**, *10*, 311. [[CrossRef](#)]
28. Montana, G. Ceramic raw materials: How to recognize them and locate the supply basins—Mineralogy, petrography. *Archaeol. Anthropol. Sci.* **2020**, *12*, 175. [[CrossRef](#)]
29. Elsen, J.; Van Balen, K.; Mertens, G. Hydraulicity in historic lime mortars: A review. *Hist. Mortars* **2012**, *7*, 125–139.
30. Bruni, S.; Cariati, F.; Fermo, P.; Pozzi, A.; Toniolo, L. Characterization of ancient magnesian mortars coming from 4 northern Italy. *Thermochim. Acta* **1998**, *321*, 161–165. [[CrossRef](#)]
31. Elsen, J. Microscopy of historic mortars—A review. *Cem. Concr. Res.* **2006**, *36*, 1416–1424. [[CrossRef](#)]
32. Margalha, G.; Veiga, R.; Silva, A.S.; De Brito, J. Traditional methods of mortar preparation: The hot lime mix methods. *Cem. Concr. Compos.* **2011**, *33*, 796–804. [[CrossRef](#)]

33. Silva, A.S.; Cruz, T.; Paiva, M.J.; Candeias, A.; Adriano, P.; Schiavon, N.; Mirão JA, P. Mineralogical and chemical characterizations of historical mortars from military fortifications in Lisbon harbour (Portugal). *Environ. Earth Sci.* **2011**, *63*, 1641–1650. [[CrossRef](#)]
34. Baragona, A.J.; Zanier, K.; Frankova, D.; Anghelone, M.; Weber, J. ARchaeometric analysis of mortars from the roman villa rustica at skolarice (Slovenia). *Ann. Anal. ZA Istrske Mediter. Stud. Ser. Hist. Et Sociol.* **2022**, *32*, 499–522.
35. Moropoulou, A.; Bakolas, A.; Bisbikou, K. Characterization of ancient, byzantine and later historic mortars by thermal and X-ray diffraction techniques. *Thermochim. Acta* **1995**, *269*, 779–795. [[CrossRef](#)]
36. Moropoulou, A.; Bakolas, A.; Moundoulas, P.; Aggelakopoulou, E.; Anagnostopoulou, S. Strength development and lime reaction in mortars for repairing historic masonries. *Cem. Concr. Compos.* **2005**, *27*, 289–294. [[CrossRef](#)]
37. Moropoulou, A.; Polikreti, K.; Bakolas, A.; Michailidis, P. Correlation of physicochemical and mechanical properties of historical mortars and classification by multivariate statistics. *Cem. Concr. Res.* **2003**, *33*, 891–898. [[CrossRef](#)]
38. Maravelaki-Kalaitzaki, P.; Bakolas, A.; Moropoulou, A. Physico-chemical study of Cretan ancient mortars. *Cem. Concr. Res.* **2003**, *33*, 651–661. [[CrossRef](#)]
39. Bakolas, A.; Biscontin, G.; Moropoulou, A.; Zendri, E. Characterization of structural byzantine mortars by thermogravimetric analyses. *Thermochim. Acta* **1998**, *321*, 151–160. [[CrossRef](#)]
40. Robert, F.; Colina, H. The influence of aggregates on the mechanical characteristics of concrete exposed to fire. *Mag. Concr. Res.* **2009**, *61*, 311–321. [[CrossRef](#)]
41. Jedrzejewska, H. Old mortars in Poland: A new method of investigation. *Stud. Conserv.* **1960**, *5*, 132–138. [[CrossRef](#)]
42. Casadio, F.; Chiari, G.; Simon, S. Evaluation of binder/aggregate ratios in archaeological lime mortars with carbonate aggregate: A comparative assessment of chemical, mechanical and microscopic approaches. *Archaeometry* **2005**, *47*, 671–689. [[CrossRef](#)]
43. Borsoi, G.; Silva, A.S.; Menezes, P.; Candeias, A.; Mirão, J. Analytical characterization of ancient mortars from the archaeological roman site of Pisões (Beja, Portugal). *Constr. Build. Mater.* **2019**, *204*, 597–608. [[CrossRef](#)]
44. Dilaria, S.; Secco, M.; Ghiotto, A.R.; Furlan, G.; Giovanardi, T.; Zorzi, F.; Bonetto, J. Early exploitation of Neapolitan pozzolan (*pulvis puteolana*) in the Roman theatre of Aquileia, Northern Italy. *Sci. Rep.* **2023**, *13*, 4110. [[CrossRef](#)] [[PubMed](#)]
45. Dilaria, S.; Secco, M.; Rubinich, M.; Bonetto, J.; Miriello, D.; Barca, D.; Artioli, G. High-performing mortar-based materials from the late imperial baths of Aquileia: An outstanding example of Roman building tradition in Northern Italy. *Geoarchaeology* **2022**, *37*, 637–657. [[CrossRef](#)]
46. Coutelas, A. *L'hydraulicité des mortiers antiques, entre préconçus et réalité: L'exemple des mortiers de tuileau et autres matériaux de Gaule romaine. Mortiers et Hydraulique en Méditerranée Antique*; Presses universitaires de Provence: Provence, France, 2019; pp. 17–30.
47. Daniele, D.; Corrado, G. Marmo e calcite spatca di vena: Termini di un equivoco sull'intonaco vitruviano. In *Annali della Scuola Normale Superiore di Pisa. Classe di Lettere e Filosofia*; Scuola Normale Superiore: Pisa, Italy, 1996; Volume 1, pp. 541–548.
48. Dilaria, S.; Sebastiani, L.; Salvadori, M.; Secco, M.; Flaviana, O.; Artioli, G. Caratteristiche dei pigmenti e dei tectoria ad Aquileia: Un approccio archeometrico per lo studio di frammenti di intonaco provenienti da scavi di contesti residenziali aquileiesi (II sec. aC-V sec. dC). In *La Peinture Murale Antique: Méthodes et Apports d'une Approche Technique*; Edizioni Quasar: Rome, Italy, 2021; pp. 125–148.
49. Lanzón, M.; Madrid-Balanza, M.J.; Martínez-Peris, I.; García-Vera, V.E.; Navarro-Moreno, D. Roman wall paintings from the Roman Forum district of Carthago Nova: Characterisation of mortars and pigments. *Constr. Build. Mater.* **2023**, *408*, 133543. [[CrossRef](#)]
50. Akyol, A.A. Material Characterization of Ancient Mural Paintings and Related Base Materials: A Case Study of Zeugma Archaeological Area. Ph.D. Thesis, Middle East Technical University, Ankara, Turkey, 2009.
51. Carneiro, A.M.S.P.; Departamento História/Laboratório de Arqueologia, Universidade de Évora, Évora, Portugal. Personal communication, 2018.
52. Fulford, M.; Jean-Pierre, A. *Roman Building: Materials and techniques*; Routledge: London, UK, 2005.
53. Bernard, E.; Nguyen, H.; Kawashima, S.; Lothenbach, B.; Manzano, H.; Provis, J.; Scott, A.; Unluer, C.; Winnefeld, F.; Kinnunen, P. MgO-based cements—Current status and opportunities. *RILEM Tech. Lett.* **2023**, *8*, 65–78. [[CrossRef](#)]
54. Pahlavan, P. *Conservation and Restoration of Historic Mortars and Masonry Structures*; Springer: Berlin/Heidelberg, Germany, 2023.
55. Dilaria, S.; Secco, M.; Bonetto, J.; Ricci, G.; Artioli, G. Making Ancient Mortars Hydraulic. How to Parametrize Type and Crystallinity of Reaction Products in Different Recipes. In *Historic Mortars International Conference*; Springer Nature: Cham, Switzerland, 2022.
56. Gonçalves, F.; Fernandes, A.P. *Carta Geológica de Portugal na Escala de 1: 50 000: Notícia Explicativa da Folha, 32-B: Portalegre*; Universitat de Barcelona: Bareselona, Spain, 1973.
57. Ditta, A. Conservation of Architectural Heritage: Characterization and Provenance of Roman Mortars. Master's Thesis, University of Évora, Évora, Portugal, 2017.

Disclaimer/Publisher's Note: The statements, opinions and data contained in all publications are solely those of the individual author(s) and contributor(s) and not of MDPI and/or the editor(s). MDPI and/or the editor(s) disclaim responsibility for any injury to people or property resulting from any ideas, methods, instructions or products referred to in the content.